Anonymous Referee #2

Received and published: 18 September 2019

Authors' response: Thank you to Anonymous Referee #2 for the kind summary and insightful questions. We appreciate the time in reviewing our manuscript and have made point-to-point responses to each question in blue text below.

Summary: The authors applied the recently developed annular denuder system (ADS) to the collection of HONO and NOx during the FIREX laboratory burns in 2016. They compare measurements of HONO across five different methods, showing decent agreement and suggesting good collection efficiency in the ADS method. Values were presented for d15N-NOx, d15N-HONO, d18O-HONO, d15N-pNO3-, and d18O-pNO3-. Some of these values compared favorably with previous measurements, and others were the first of their kind. I found this manuscript to be well written. I recommend it for publication after some minor corrections and explanations.

Specific Comments:

Abstract: I personally find that your abstract is too broad. In the first two paragraphs, there is a lot of text about describing the methods, and the real results of your work are getting buried in the later paragraphs. I think you could increase the impact of your work by removing some of the general statements and focusing on specific results (numbers and direct conclusions) as described in the latter two paragraphs.

Thank you, the abstract has been modified following the reviewer's suggestions.

Pg 5 Ln 152-153: How did you decide on the acronyms/abbreviations for each fuel type? Most of them don't seem to make any intuitive sense, and this is very distract- ing when trying to understand your results. I'd recommend you make them easier to understand, e.g., Douglas-fir (DFIR), etc.

Authors' response: Thank you for the suggestion! The acronyms are defined based on Latin names of the vegetation species, as you can see in this example (https://plants.usda.gov/core/profile?symbol=PICO)

For readers' convenience, all the acronyms have been replaced by corresponding names.

Pg 6 Ln 225: I have several questions regarding this section about the NOx measure- ments: a) Throughout the manuscript, whenever you give NOx values or use NOx values in calculations, are you using the values from the collection of NOx after the ADS system, or are you using NOx values measured using the Thermo instrument? My impression is that you always use the former, and never show any data from the Thermo instrument. If so, you really have no reason to mention the Thermo measurement at all here, and it could be removed. (If not, then please be explicit throughout the manuscript about where the NOx data originated at each mention in the text). b) However, I don't

suggest you remove the description of the Thermo instrument! Instead, I suggest you show the data that underlies the statement "The NOx measurement verified the concentration of the NOx collected for isotopic analysis, and the original NOx data is available. . ." This would be a plot analogous to Fig. 3 but for NOx, potentially in a new section analogous to Sect 3.2 (or in the SI, in which case the Thermo instrument description should also move there).

Authors' response:

Thanks for bring up this question and the suggestion! The NOx concentrations we used in discussion are all from the NOx collection system, as it offers a direct comparison with HONO concentration in the same system. The NOx analyzer measurement is used to verify the NOx collected with our collection system and the original 1-minute time resolution data is stored in NOAA archive. Since the NOx collection method has been validated in both lab and field previously (Fibiger et al., 2014, Fibiger and Hastings, 2016), we did not expand it in this manuscript. Apologies for the confusion. Based on the reviewer's suggestion, we add Table S1 and Figure 1S to show the comparison of [NOx_collected] versus [NOx_analyzer], in addition to moving the NOx analyzer description to supplemental information. Please note that each NOx concentration recovered from the collection system represents mean concentration across each whole fire, and therefore the [NOx_analyzer] concentrations used for the comparison are a mean value across the whole fire.

Pg 6 Ln 234-237: How important is the interference of HONO on the Thermo NOx instrument? Please provide more information about how you corrected for it (e.g., what fraction of HONO did you assume gets converted to NO in the catalyst?), and provide the numbers for how large the correction was relative to the total NOx measurement. At this point, you only mention the correction in passing, and a reader cannot determine how important the correction is.

Authors' response:

Thank you for asking this question. HONO is an important interference with NO2 using the chemiluminescence analyzer. We correct the NOx concentration by subtracting mean HONO concentration during each fire from NOx concentration by assuming HONO is 100% converted to NO on Molybdenum catalyst (e.g. Febo et al 1995), and this provided an approximate lower limit of NOx concentration. The following text is added to the description section of the NOx analyzer, which is now moved to SI.

"In this study, only the HONO interference was corrected for. This was done by subtracting the ADS measured HONO concentration (mean value across each whole fire) from Thermo analyzer measured NO_x concentration averaged across the whole fire; this provided the approximate lower limit of the NO_x concentration by assuming HONO is 100% converted to NO on the Molybdenum catalyst (e.g. Febo et al 1995)."

Pg 9 Ln 330: It should be mentioned somewhere here that the PTR-ToF is a mass spectrometer. It is important for consistency that you also use the same acronym for the

instrument as they use in the cited Koss and Yuan papers.

Authors' response:

Thanks for the suggestions. The PTR-ToF mass spectrometer is briefly described in the next sentence following Ln 330.

Pg 10 Ln 394: Your HONO/NOx ratios were calculated as averages across the entire burn, correct? This is good for comparison to previous results, but I'm wondering if you can also calculate a time dependent HONO/NOx ratio across each burn. In other words, as each burn transitions from flaming to smoldering, does this HONO/NOx ratio change? This would be important to note for real wildfires that may have different ratios of flaming vs smoldering emissions.

Authors' response:

This is a very interesting comment! HONO/NOx ratios reported here are based on the concentrations collected in our HONO and NOx collection train. The time resolution of our data is over the whole fire period; similarly, MCE values (from CO and CO2) are also reported by fire (in the NOAA FIREX Firelab data archive). The primary focus of this manuscript is isotopic composition analyses of reactive nitrogen species from biomass burning, and the higher time resolution HONO/NOx ratio vs MCE could be an interesting topic for future work. Lastly, since both HONO and NOx are favored by flaming combustion condition, we would not expect to see a strong trend of the relation between HONO/NOx vs MCE.

Pg 14 Ln 567: This line suggests that the average combustion temperature was "moderate" (e.g. 700C) rather than high temp (>850C). How does that translate to flaming vs smoldering? What is a typical temperature for each phase? More specifically, my question is are you saying that the flaming during FIREX was typically closer to 700C than 850C, or are you saying that flaming could have been near the hotter end of the spectrum but the dominant source of emissions was from smoldering processes at lower temp?

Authors' response:

Great questions. Our results do not suggest the average combustion temperature was "moderate" (e.g. 700C) rather than high temp (>850C); instead, our results only suggest R1-R6 occurred to a larger extent than R7-R11 (percentage can be used as an analogy). If R1-R6 is dominant over R7-R11, or say R7-R11 is negligible, R1-R6 would result in much larger isotopic effect, leading to much larger δ^{15}N-NO_x than δ^{15}N-HONO (e.g. by >10‰) instead of the small difference observed here (Figure 4 and Figure 6). … Biomass combustion temperature ranges from 200°C—1200°C with flaming at 1000-1200°C, glowing at ~800°C and smoldering <600°C, and the temperature changes as fire progresses. Many fires are mixtures of flaming and smoldering, and therefore we do not intend to infer flaming or smoldering with our comparison of δ^{15}N-NO_x with δ^{15}N-HONO. Rather, this comparison suggests a source signature that could be used to track

wildfire emission and its aging process in the atmosphere.

General comment: Related to my previous comment, can you add a few sentences (perhaps in the conclusions section) about how exactly your measurements of fresh lab smoke may relate to measurements of fresh wildfire smoke? You've given some discussion about how you expect the d15N-HONO and d15N-NOx to depend on combustion temperature, and in wildfires you are likely to have instances where the (average) combustion temperature is potentially very different than what you measured in the lab. To my understanding, there is currently no good way of determining exact combustion temperatures either in the lab or in the field, so I'm not asking you to solve this problem but rather to acknowledge it and provide some guidance for how future isotopic measurements in wildfires could be interpreted relative to your results.

Authors' response:

We agree with the reviewer regarding this point. In addition to our response to the previous question, we have modified original text in the conclusion section to now read as follows (Ln 640-649):

"The relationship between δ^{15}N-HONO and δ^{15}N-NO_x likely reflects that HONO was produced to a larger extent at moderate combustion temperatures (< ~800 °C) than higher temperatures on the basis of a simplified mechanism for flow of reactive nitrogen species. However, we note that this relationship is derived from all measured δ^{15}N-HONO and δ^{15}N-NO_x in fires ranging from smoldering to flaming, so is not necessarily representative of a particular combustion condition. Still, it is likely that a compilation over a range of conditions is more useful for potentially distinguishing HONO sources and formation pathways in the environment since it will always be a challenge to assess exact combustion temperatures."

Figure 3: Please change the "CIMS" label in the legend to match the "PTR-ToF" designation in the caption.

"PTR-ToF" has been put in the legend to replace "CIMS".

Isotopic characterization of nitrogen oxides (NO_x), nitrous acid (HONO), and nitrate (NO_3^-(p)) from laboratory biomass burning during FIREX

Jiajue Chai[1], David J. Miller[1,a], Eric Scheuer[2], Jack Dibb[2], Vanessa Selimovic[3], Robert Yokelson[3], Kyle J. Zarzana[4,5,b], Steven S. Brown[4,6], Abigail R. Koss[4,5,6,c], Carsten Warneke[5,6], Meredith Hastings[1]

1. Department of Earth, Environmental and Planetary Sciences, and Institute at Brown for Environment and Society, Brown University, Providence, RI, USA
2. Institute for the Study of Earth, Ocean and Space, University of New Hampshire, Durham, NH, USA
3. Department of Chemistry, University of Montana, Missoula, USA
4. Chemical Sciences Division, NOAA Earth System Research Laboratory, Boulder, CO, USA
5. Cooperative Institute for Research in Environmental Sciences, University of Colorado, Boulder, CO, USA
6. Department of Chemistry, University of Colorado, Boulder, CO, USA

a. Now at: Environmental Defense Fund, Boston, MA, USA
b. Now at: Department of Chemistry, University of Colorado, Boulder, CO, USA
c. Department of Civil and Environmental Engineering, Massachusetts Institute of Technology, Cambridge, MA, USA

Correspondence: Jiajue Chai (jiajue_chai@brown.edu)

Abstract

New techniques have recently been developed and applied to capture reactive nitrogen species including nitrogen oxides (NO_x = NO + NO_2), nitrous acid (HONO), nitric acid (HNO_3) and particulate nitrate (NO_3^-(p)), for accurate measurement of their isotopic composition. Here, we report – for the first time – the isotopic composition of HONO from biomass burning (BB) emissions collected during the Fire Influence on Regional to Global Environments Experiment (FIREX, later evolved into FIREX-AQ) laboratory experiments at the Missoula Fire Science Laboratory in the fall of 2016. Using our newly developed annular denuder system (ADS), which was verified to completely capture HONO associated with BB via comparison with 4 other high time resolution concentration measurement techniques, including mist chamber/ion chromatography (MC/IC), open-path Fourier transform infrared spectroscopy (OP-FTIR), cavity enhanced spectroscopy (CES), and proton-transfer-reaction time-of-flight mass spectrometer (PTR-ToF).

In 20 "stack" fires (direct emission within ~5 seconds of production by the fire) that burned various biomass materials from the Western U.S., δ^{15}N-NO_x ranges from -4.3 ‰ to +7.0 ‰, falling near the middle of the range reported in previous work. The first measurements of δ^{15}N-HONO and δ^{18}O-HONO in biomass burning smoke reveal a range of -5.3‰ to +5.8‰ and +5.2‰ to +15.2‰, respectively. Both HONO and NO_x are sourced from N in the biomass fuel and δ^{15}N-HONO and δ^{15}N-NO_x are strongly correlated (R^2 = 0.89, $p<0.001$), suggesting HONO is directly formed via subsequent chain reactions of NO_x emitted from biomass combustion. Only 5 of 20 NO_3^-(p) samples had a sufficient amount for isotopic analysis, and showed δ^{15}N and δ^{18}O of NO_3^-(p) range from -10.6‰ to -7.4 ‰ and +11.5‰ to +14.8‰ respectively.

Our δ^{15}N of NO_x, HONO and NO_3^-(p) ranges can serve as important biomass burning source signatures, useful for constraining emissions of these species in environmental applications. The δ^{18}O of HONO and NO_3^- obtained here verify our method is capable of determining the oxygen isotopic composition in BB plumes. The δ^{18}O for both of these species reflect laboratory conditions (i.e. a lack of photochemistry), and would be expected to track with the influence of different oxidation pathways in real environments. The methods used in this study will be further applied in future field studies to quantitatively track reactive nitrogen cycling in fresh and aged Western US wildfire plumes.

1 Introduction

Biomass burning (BB), which occurs in both anthropogenic processes (e.g. cooking, heating, and prescribed burning that is human controlled burning for management purpose) and natural wildfire (lightning ignited vegetation burning), is a significant source of atmospheric reactive nitrogen species, including nitrogen oxides (NO_x = NO + NO_2), nitrous acid (HONO), nitric acid (HNO_3), particulate nitrate (NO_3^-(p)), organic nitrates, peroxyacyl nitrate (PAN) and ammonia (NH_3) that have major impacts on air quality and climate from regional to global scales (Crutzen and Andreae, 1990). Globally, biomass burning emits ~6 Tg of nitrogen oxides (NO_x = NO + NO_2) per year, contributing at least 14% to total NO_x emissions (Jaeglé et al., 2005), with large interannual and seasonal variation due to fire frequency and intensity (Jaffe and Briggs, 2012). Primarily emitted NO_x plays an important role in the photo-oxidation of volatile and semi volatile organic compounds, which are present in high concentrations in BB plumes, and strongly influences production of tropospheric ozone (O_3) and secondary aerosols (Alvarado et al., 2015). In BB plumes, NO_x can be converted to PAN, which can be transported long distances (100s to 1000s of km) in lofted plumes before rereleasing NO_x. Therefore, BB emitted NO_x could widely influence air quality downwind for days to weeks (Val Martín et al., 2006; Ye et al., 2016). In addition, NO_x is also the major photochemical precursor of HNO_3 and NO_3^-(p), which can be transported downwind, mix with anthropogenic emissions, and impact air quality and ecosystem health (Hastings et al., 2013).

HONO has been observed in BB plumes in both laboratory and field experiments, with HONO mixing ratios in the range of ~5-33% of observed NO_x (Akagi et al., 2012, 2013; Burling et al., 2010, 2011; Keene et al., 2006; Liu et al., 2016; Roberts et al., 2010; Selimovic et al., 2018; Yokelson et al., 2007, 2009). Photolysis of HONO is a major OH precursor in the daytime; therefore HONO plays an important role in photochemical aging of BB plumes and atmospheric oxidation capacity at regional scales (Alvarado and Prinn, 2009; Liu et al., 2016; Tkacik et al., 2017; Trentmann et al., 2005). HONO has been proposed as a significant OH source in BB plumes and the inclusion of HONO in photochemical models could explain much of the uncertainty in the modeled O_3 (Alvarado et al., 2009; Alvarado and Prinn, 2009; Cook et al., 2007; Travis et al., 2016; Trentmann et al., 2005).

Direct BB emission factor measurements of HONO and NO_x exhibit significant uncertainties due to limited observations and large spatial and temporal variability of burning conditions, making it challenging to build an accurate inventory of BB emissions relative to other major sources (Lapina et al., 2008). Emission factors vary and mainly depend on 1) fuel nitrogen content (0.2 – 4% by mass), which is a function of vegetation type, and 2) modified combustion efficiency (MCE = $\Delta[CO_2]/(\Delta[CO] + \Delta[CO_2])$ that is determined by combustion conditions including fuel moisture, fuel load, temperature, relative humidity, wind speed, and other meteorological parameters (Burling et al., 2010; Jaffe and Briggs, 2012; Yokelson et al., 1996). Additionally, the temporal evolution of HONO in BB plumes varies greatly in different fires and relative contributions from direct emission versus NO_2 conversion to HONO remains unclear. For instance, significant concentrations of HONO and correlation between HONO and NO_2 have been observed in aged plumes, indicating the importance of heterogeneous conversion of NO_2–

to–HONO on BB aerosols (Nie et al., 2015). By contrast, no evidence was found for secondary HONO formation in a BB plume during the Southeast Nexus Experiment (Neuman et al., 2016). It is important to constrain HONO directly emitted from BB compared to HONO formed during plume aging. This would reduce uncertainties associated with the total HONO budget and increase our understanding of HONO impacts on O_3 and secondary aerosol formation downwind of BB regions.

In an effort to better understand reactive nitrogen emissions and chemistry, especially for HONO, new techniques have been developed to analyze the isotopic composition of various species. Stable isotopes provide a unique approach of characterizing and tracking various sources and chemistry for a species of interest (Hastings et al., 2013). Fibiger et al. (2014) developed a method to quantitatively collect NO_x in solution as NO_3^- for isotopic analysis, which has been verified to avoid any isotopic fractionation during collection in both lab and field studies. This allows for high-resolution measurement of $\delta^{15}N\text{-}NO_x$ in minutes to hours depending on ambient NO_x concentrations ($\delta^{15}N = [(^{15}N/^{14}N)_{sample}/(^{15}N/^{14}N)_{air\text{-}N2} - 1] \times 1000‰$, and $\delta^{18}O = [(^{18}O/^{16}O)_{sample}/(^{18}O/^{16}O)_{VSMOW} - 1] \times 1000‰$ where VSMOW is Vienna Standard Mean Ocean Water). $\delta^{15}N$ has also been used to track gaseous NO_x from a variety of major sources including emissions from biomass burning (Fibiger and Hastings, 2016), vehicles (Miller et al., 2017), and agricultural soils (Miller et al., 2018). Using this method, Fibiger and Hastings (2016) systematically investigated BB $\delta^{15}N\text{-}NO_x$ from different types of biomass from around the world in a controlled environment during the fourth Fire Lab at Missoula Experiment (FLAME-4). NO_x emissions collected both immediately from the BB source and 1-2 hours after the burn in a closed environment ranged from -7 to +12‰, and primarily depended on the $\delta^{15}N$ of the biomass itself. BB emitted HONO isotopic composition has never been measured before. Our recently developed method for HONO isotopic composition analysis (Chai and Hastings, 2018) enables us to not only characterize $\delta^{15}N$ and $\delta^{18}O$ of HONO, but also explore the connection between $\delta^{15}N\text{-}NO_x$ and $\delta^{15}N\text{-}HONO$.

The Fire Influence on Regional to Global Environments and Air Quality (FIREX-AQ) investigates the influence of fires in the western U.S. on climate and air quality, via an intensive, multi-platform, campaign. The first phase of FIREX-AQ took place at the US Forest Service Fire Sciences Laboratory (FSL) in Missoula, Montana, in the fall of 2016, where we measured $\delta^{15}N\text{-}NO_x$, $\delta^{15}N\text{-}HONO$, $\delta^{18}O\text{-}HONO$, $\delta^{15}N\text{-}NO_3^-(p)$, $\delta^{18}O\text{-}NO_3^-(p)$ and $\delta^{15}N$-biomass in 20 “stack burns” of a variety of fuels representative of northwestern North America. Here we report on the results and explore relationships between the isotopic composition of these reactive nitrogen species, as well as the corresponding mixing ratios for HONO that were concurrently measured by a variety of techniques. This work offers characterization and quantification of BB source signatures of these species, which can be applied in the interpretation of observations in future field studies.

2. Experimental details

2.1 FIREX Fire Science Laboratory design

The room for controlled BB experiments is 12.5 × 12.5 m × 22 m, with a continuously weighed fuel bed at the center of the room. The combustion exhaust was vented at a constant flow rate (~3.3 m s^{-1}) through a 3.6 m diameter inverted funnel followed by a 1.6 m diameter stack, and collected at a platform 17 m above the fuel bed via sampling ports that surround the stack, resulting in a transport time of ~5 s. Further details have been described in the literature (Stockwell et al., 2014). All of our instruments for sampling and online measurements were placed on the platform, which can accommodate up to 1820 kg of equipment and operators. Measurements were focused on the "stack burns", for which fires lasted a few minutes up to 40 minutes.

For this study, we investigated 20 stack fires of vegetation types abundant in the western US, representing coniferous ecosystems, including ponderosa pine (PIPO), lodgepole pine (PICO), Engelmann spruce (PIEN), Douglas-fir (PSME) and subalpine fir (ABLA), with replicate burns for most of these types (Table 1). Some of the fires proceeded by burning of an individual fuel component such as litter, canopy, duff and rotten logs. Other fires simulated actual biomass in the coniferous ecosystem by mixing various fuel components in realistically recreated ecosystem matrices using the first order fire effects model (FOFEM) (Reinhardt et al., 1997).

2.2 Instrumentation

2.2.1 Collection of HONO, NO_x and nitrate for isotopic analysis

HONO was completely collected for isotopic analysis using an annular denuder system (ADS) (Chai and Hastings, 2018). The ADS system deployed in this laboratory experiment consisted of a Teflon particulate filter, a Nylasorb filter to remove HNO_3, followed by two annular denuders, each coated with a solution of 10 mL of Na_2CO_3 (1% w/v) + glycerol (1% v/v) + methanol−H_2O solution (1:1 volume ratio) following a standard EPA method. Methanol and glycerol are certified ACS plus with a purity of ≥99.8% and ≥99.5%, respectively. After coating, the denuders are dried using zero air and capped immediately. Within 6 hours after each collection, the coating was extracted in 10 mL of ultrapure water (18.2 MΩ) in two sequential 5 mL extractions. The extracted solution with a pH of ~10 was transported to Brown University for concentration and isotopic analysis 3-14 days after the sampling. The timescales for sample extraction and isotopic analysis preserve both the solution concentration and isotopic composition of HONO in the form of nitrite (Chai and Hastings, 2018). The two-denuder set up allows us to minimize the interference for both concentration and isotopic analysis from other N-containing species that could be trapped and form nitrite in residual amounts on the denuders, especially NO_2. Our method development study showed NO_2 tends to absorb in the same amount (difference <4%) on the walls of each denuder in a train setup, which is consistent with other studies (Perrino et al., 1990; Zhou et al., 2018). On the basis of this validation, the second denuder extract is used to correct the first denuder extract for both concentration and isotopic composition (Chai and Hastings, 2018). Note HONO levels

were above the minimum detection limit (0.07 μM) and the breakthrough amount of HONO threshold is far from being reached given the concentrations (Table 1), flow rate (~ 4 L/min) and collection times (5 - 40 min). The necessary minimum amount of nitrite collected for isotopic analysis is 10 - 20 nmol.

To avoid scrubbing of HONO, a flow meter (Omega) and the NO_x collection system for analysis of $\delta^{15}N\text{-}NO_x$ are placed following the ADS (Fibiger et al., 2014; Fibiger and Hastings, 2016; Wojtal et al., 2016). In brief, NO_x is collected in a solution containing 0.25 M $KMnO_4$ and 0.5 M NaOH which oxidizes NO and NO_2 to NO_3^- by pumping sampled air through a gas washing bottle with a 65 Watts diaphragm vacuum pump. The flow rate (~4L/min with ±1% uncertainty) is controlled with a critical orifice inserted between the pump and gas stream outlet, and is monitored and recorded with a flow meter placed prior to the NO_x collector. The NO_x trapping solution blanks are also collected every day to quantify background NO_3^- for concentration and isotopic blank corrections. The Omega flow meter was calibrated with another flow meter (Dry Cal Pro) by varying flow rates. Within a day after collection, we stabilized the samples in the wet chemistry lab in the Fire Science Lab by adding 30% w/w H_2O_2 that reduces MnO_4^- to MnO_2 precipitate before being shipped back to Brown University for further processing. This effectively excludes the possible interferences from NH_3 that could be oxidized to NO_3^- by MnO_4^- after a week (Miller et al. (2017) and references therein). The samples were neutralized with 12.1 N HCl in the Brown lab, before concentration measurement and isotopic analyses. NO_3^- on the upstream Millipore filters and HNO_3 from the Nylasorb filters, if there was any, were extracted by sonicating the filters in ~30 mL ultrapure H_2O (18.2 MΩ) for 30 minutes. Samples with $[NO_3^-] > 1$ μM were analyzed for isotopic composition (concentration techniques detailed below).

All treated samples from both HONO collection and NO_x collection and their corresponding blanks were analyzed offline for concentrations of NO_2^- and NO_3^- with a WestCo SmartChem 200 Discrete Analyzer colorimetric system. The reproducibility of the concentration measurement was ±0.3 μmol L^{-1} (1σ) for NO_2^- and ±0.4 μmol L^{-1} for NO_3^- when a sample was repeatedly measured (n = 30). A detection limit of 0.07 μmol L^{-1} for NO_2^- and 0.1 μmol L^{-1} for NO_3^- was determined, and no detectable nitrite or nitrate was found in the blank denuder coating solution, whereas blank NO_3^- concentrations of ~5 μM are typical for the NO_x collection method (Fibiger et al., 2014; Wojtal et al., 2016). Note that NO_3^- concentration was measured on the ADS solutions to verify whether and to what extent NO_2^- was oxidized to NO_3^- on denuder walls because the denitrifier method converts both NO_3^- and NO_2^- to N_2O for isotopic analysis (see below). In addition, samples collected with a mist chamber/ion chromatography system (described in Sect. 2.2.2) were also tested for their concentrations and only those with sufficient nitrite quantity were further analyzed for isotopic composition.

2.2.2 NO_x and HONO online concentration measurement

NO and NO_x concentrations were measured with a Thermo Scientific Model 42i chemiluminescence NO/NO_x analyzer, which is described in supplemental information. The NO_x measurement verified the concentration of the NO_x collected for isotopic analysis, shown in Table S3 and Figure S1.

HONO and HNO_3 concentrations were measured using the University of New Hampshire's dual mist chamber/ion chromatograph system (Scheuer et al., 2003) with the sampling inlet placed right next to that of the ADS. The dual channel IC system is custom built using primarily Dionex analytical components. Briefly, automated syringe pumps are used to move samples and standard solutions in a closed system, which minimizes potential contamination. A concentrator column and 5 ml injections were used to improve sensitivity. Eluents are purged and maintained under a pressurized helium atmosphere. Background signal is minimized using electronic suppression (Dionex-ASRS). The chromatography columns and detectors are maintained at 40 °C to minimize baseline drifting. A tri-fluoro-acetate tracer spiked into the ultra-clean sampling water is used as an internal tracer of sample solution volume, which can decrease due to evaporation in the exhaust flow by 10-20% depending on the ambient conditions and length of the sample integration interval. The spike was analyzed to correct the final mist chamber sampled solution volume with an uncertainty of ±3%. This system has been deployed to various field studies for HONO measurement (Dibb et al., 2002; Stutz et al., 2010) and showed reasonable intercomparison with other HONO measurement techniques (within 16% uncertainty) during the 2009 SHARP campaign in Houston (Pinto et al., 2014). The detection limits for HNO_3 and HONO are 10 ppt for 5-minute sample integrations. During the experiments, two mist chambers were operated to collect gas samples in parallel, each with an integration interval of 5 minutes. One channel of the IC was utilized for concentration measurement; in the other, the mist chamber's solution was transferred into a sample bottle using the syringe pump, and the collected solution was brought to Brown University for isotopic analysis of HNO_3 if sufficient amount (10-20 nmol) was collected for each sample.

In addition to MC/IC, the HONO mixing ratios were also measured using high time-resolution (~1 second) measurement techniques including open-path Fourier transform infrared spectroscopy (OP-FTIR) (Selimovic et al., 2018), cavity enhanced spectrometer (CES) (Min et al., 2016; Zarzana et al., 2018), and proton-transfer-reaction time-of-flight mass spectrometer (PTR-ToF). Inlet ports of CES and PTR-ToF were placed 5' apart from, but at the same height on the platform as those for ADS and MC/IC, while the OP-FTIR had an open path cell at the stack. The smoke has been shown to be well-mixed at the sampling platform (Christian et al., 2004) and the mean HONO mixing ratios across each fire obtained from the four techniques were compared with that retrieved from ADS collection. This offers comprehensive verification of complete capture of HONO by ADS that is extremely important for conserving the isotopic composition of HONO.

The details of OP-FTIR are described in previous works (Selimovic et al., 2018; Stockwell et al., 2014). The setup included a Bruker MATRIX-M IR cube spectrometer with a mercury cadmium telluride (MCT) liquid-nitrogen-cooled detector interfaced with a 1.6 m base open-path White cell. The white cell was positioned on the platform and its open path spanned the width of the stack. This facilitates direct measurement across the rising emissions. The optical path length was set to 58 m. The IR spectra resolution was 0.67 cm^{-1} from 600–4000 cm^{-1}. Pressure and temperature were continuously recorded with a pressure transducer and two temperature sensors respectively, which were placed adjacent to the White cell optical path. They were used for spectral analysis. Time resolution for stack burns was approximately 1.37 s. The OP-FTIR measures CO_2, CO,

CH_4, a series of volatile organic compounds and various reactive nitrogen species (Selimovic et al., 2018). Mixing ratios of HONO were retrieved via multicomponent fitting to a section of the mid-IR transmission spectra with a synthetic calibration nonlinear least-squares method (Griffith, 1996; Yokelson et al., 2007), and both the HITRAN spectral database and reference spectra recorded at the Pacific Northwest National Laboratory (Rothman et al., 2009; Sharpe et al., 2004; Johnson et al., 2010, 2013) were used for the fitting. The uncertainty is ~10% for the HONO mixing ratio measurement and the detection limit is no more than a few ppb as reported in previous studies (Stockwell et al., 2014; Veres et al., 2010).

HONO measurements by cavity enhanced spectroscopy used the airborne cavity enhanced spectrometer, ACES, recently described by Min *et al.* (2016). This instrument consists of two channels, one measuring over the spectral range from 438-468 nm where glyoxal (CHOCHO) and NO_2 have structured absorption bands, and one measuring over from 361-389 nm, where HONO has structured absorption. In the HONO channel, light from an LED centered at 368 nm and with an output power of 450 mW and collimated with an off-axis parabolic collector illuminates the input mirror of a 48 cm optical cavity formed from mirrors with a maximum reflectivity R = 99.98% at 375 nm. The effective path length within the optical cavity is > 3 km over the region of greatest reflectivity. The mirror reflectivity (effective path length) was calibrated from the difference in Rayleigh scattering between Helium and zero air to provide an absolute calibration of the instrument response. A fiber optic bundle collects light exiting the optical cavity and transmits it to a grating spectrometer with a CCD detector, where it is spectrally dispersed at a resolution of 0.8 nm. The resulting spectra are fit using DOASIS software (Kraus, 2006) to determine trace gas concentrations, including NO_2, HONO and O_4. Mixing ratios of NO_2 and HONO are reported at 1 s resolution, although the NO_2 precision is higher in the 455 nm channel. The 1 Hz HONO precision is 800 pptv (2σ). (The precision of the HONO instrument in ACES is somewhat degraded by the optimization of 455 nm channel for glyoxal detection, which reduces the photon count rate on the 368 nm channel.) The accuracy of the HONO measurement is 9%. Air was sampled directly from stack at a height of 15 m above the fuel bed through a 1 m length of ¼" O.D. Teflon (FEP) tubing as described in Zarzana *et al.* (2018). The residence time in the inlet and sample cells was < 1 s. Comparison between the ACES HONO and an open path FTIR agreed to within 13% on average, and ACES HONO was well correlated with 1Hz measurements from a PTR-ToF ($r^2 = 0.95$) (Koss et al., 2018).

The PTR-ToF instrument used in the FIREX Fire Lab experiment is described in detail in previous studies (Koss et al., 2018; Yuan et al., 2016). The PTR-ToF instrument is a chemical ionization mass spectrometer typically using H_3O^+ reagent ions and a wide range of trace gases can be detected in the range of tens to hundreds of parts per trillion (pptv) for a 1 s measurement time. At the Fire Lab, PTR-ToF detected several inorganic species including HONO with an uncertainty of 15%. HONO is detected at a lower sensitivity than most trace gases in PTR-ToF, but mixing ratios for all fires were well above the detection limit.

2.2.3 Isotopic composition measurements

The denitrifier method was used to perform nitrogen and oxygen isotope analyses ($^{15}N/^{14}N$, $^{18}O/^{16}O$) of NO_3^- and/or NO_2^-, by complete conversion to N_2O by denitrifying bacteria *P. aureofaciens* (Casciotti et al., 2002; Sigman et al., 2001). The isotopic composition of N_2O is then determined by a Thermo Finnegan Delta V Plus isotope ratio mass spectrometer at *m/z* 44, 45 and 46 for $^{14}N^{14}N^{16}O$, $^{14}N^{15}N^{16}O$ and $^{14}N^{14}N^{18}O$, respectively. Sample analyses were corrected against replicate measurements of the NO_3^- isotopic reference materials USGS34, USGS35, and IAEA-NO-3 (Böhlke et al., 2003). Additional correction was performed for $\delta^{18}O$-HONO following previous studies (Casciotti et al., 2002, 2007; Chai and Hastings, 2018). Precisions for $\delta^{15}N$-HONO, $\delta^{18}O$-HONO and $\delta^{15}N$-NO_x isotopic analysis across each of the entire methods are ±0.6‰, ±0.5‰ and ±1.3‰, respectively (Chai and Hastings, 2018; Fibiger et al., 2014). $\delta^{18}O$-N_2O from the NO_x collection samples was measured but is not reported as $\delta^{18}O$-NO_x because it is greatly impacted by MnO_4^- oxidation and does not represent the $\delta^{18}O$-NO_x in the sample air. The total $\delta^{15}N$ of the starting biomass ($\delta^{15}N$-biomass) was measured at the Marine Biological Laboratory Ecosystems Center Stable Isotope Facility. The materials measured for $\delta^{15}N$-biomass (Table S1) cover most but not all the biomass types burned in the experiments depending on availability of the leftover materials. Analyses were conducted using a Europa ANCA-SL elemental analyzer−gas chromatograph preparation system interfaced with a Europa 20−20 continuous-flow gas source stable isotope ratio mass spectrometer. Analytical precision was ±0.1‰, based on replicate analyses of international reference materials.

Collection time spanned the whole fire burning (5 min to 40 min) in order to maximize the signal. We chose to report the samples whose concentrations are at least 30% above the 5 μM NO_3^- present in the blank $KMnO_4$ solution upon purchase (Fibiger et al., 2014), such that the propagated error through the blank correction does not exceed the analytical precision of ±1.5‰ for $\delta^{15}N$-NO_x. We found identical concentration and isotopic signatures for both Fire Lab and Brown University Lab blanks, which ensures that no additional NO_3^- contamination was introduced into the $KMnO_4$ solutions in the gas-washing bottle. In addition, fires with high particulate loading that resulted in >50% reduction in flow rate are not considered for isotopic analysis because the low flow rate could induce incomplete collection with potential isotopic fractionation that might not represent BB emissions.

3. Results and discussion

3.1 Temporal evolution of HONO and HNO_3 from direct BB emissions

The time series of HONO and HNO_3 concentrations measured by MC/IC at 5-minute resolution for majority of the stack burns are shown in Fig. 1, and original data can be found in the NOAA data archive (FIREX, 2016). HNO_3 concentrations were nearly two orders of magnitude lower than typical HONO concentrations. The constant low concentration of HNO_3 from fresh emissions across all fires is consistent with the findings in Keene et al. (2006), confirming HNO_3 is not a primary reactive nitrogen species in fresh smoke. Rather, it is largely produced secondarily in aged smoke and nighttime chemistry. Both HONO and HNO_3 mixing ratios reach their peak in the first five minutes, except for fire no. 12 (Engelmann spruce - duff), from which HONO

concentration remains nearly constant over the course of each fire, but much lower than HONO concentration of the rest of the fires. The largest HONO and HNO_3 were emitted from burning subalpine fir-Fish Lake canopy (fire no. 15), integrated concentration of up to 177 ppbv and 1.9 ppbv in the first 5-minute sample, respectively. We note that fires no. 12 has the smallest MCE value 0.868 (FIREX, 2016), and abnormal flow rate (less than half of the typical flow rate during all other measurements) due to the inlet filter clogging from extraordinarily large particulate loadings. In general, the closer the MCE value is to 1, the more likely N-oxidation (e.g. NO_x and HONO) dominates over N-reduction (e.g. NH_3 and HCN) as a result of flaming; when MCE approaches 0.8, more smoldering occurs such that N-reduction becomes dominant (Ferek et al., 1998; Goode et al., 1999; McMeeking et al., 2009; Yokelson et al., 1996, 2008). Accordingly, the smoldering combustion condition of fire no. 12 leads to lower concentration of oxidized nitrogen species than the rest of the fires in this study. Although fires no. 15 and no. 17 have relatively low MCE (~0.89), the pulse of HONO in first 5-10 minutes suggest an active flaming phase followed by longer smoldering phase. This indicates both fires had combustion conditions that consisted of a mixture of flaming and smoldering, and thus significant HONO was still produced. In addition, $HONO/NO_x$ ratio ranged from 0.13 to 0.53 with a mean of 0.29±0.12 (1σ), comparable with previous results of laboratory experiments (0.11±0.04) and field experiments (0.23±0.09) (Akagi et al., 2013; Burling et al., 2010, 2011)

3.2 Verification of ADS collected HONO concentration

The HONO collected with the ADS represents a mean value over the course of each entire burn. We first compare HONO concentration recovered from the ADS, denoted as $[HONO]_{ADS}$, with that measured with the collocated MC/IC when both measurements were available (Fig. 2). The comparison demonstrates good consistency across all fires, with the $[HONO]_{ADS}$ of all available fires falling within the first and third quartile of MC/IC HONO data. Additionally, we made intercomparisons between $[HONO]_{ADS}$ with mean values of various high resolution methods including MC/IC, OP-FTIR, ACES and PTR-ToF that are also available from the NOAA data archive (Fig. 3; FIREX, 2016). The mean values used for the comparison are shown in Table S2. The linear regression results for all four comparisons are:

$$[HONO]_{ADS} = (1.07\pm0.24)\,[HONO]_{MCIC} - 0.72 \quad \text{Eq. (1)}$$
($R^2 = 0.63$; $p_{slope} < 0.001$, $p_{intercept}=0.95$);

$$[HONO]_{ADS} = (1.07\pm0.08)\,[HONO]_{ACES} - 4.63 \quad \text{Eq. (2)}$$
($R^2 = 0.95$; $p_{slope} < 1\times10^{-6}$, $p_{intercept}=0.32$);

$$[HONO]_{ADS} = (1.07\pm0.22)\,[HONO]_{FTIR} + 5.48 \quad \text{Eq. (3)}$$
($R^2 = 0.75$; $p_{slope} < 0.005$, $p_{intercept}=0.48$);

$$[HONO]_{ADS} = (1.08\pm0.19)\,[HONO]_{PTR\text{-}ToF} - 8.81 \quad \text{Eq. (4)}$$
($R^2 = 0.87$; $p_{slope} < 0.005$, $p_{intercept}=0.28$).

We found significant linear correlation between each of the [HONO] techniques and [HONO] $_{ADS}$ with a slope of ~1. Note that the y-intercepts of Eq. (1)—(4) are much smaller than the overall range of measured [HONO] (up to 121 ppbv). In addition, p-values of the intercepts for all 4 fittings are much greater than 0.05, suggesting the intercepts are not significantly different from zero. All data except one fall within 95% prediction interval bounds of the overall fitting (Fig. 3). Therefore, we conclude that the ADS method has high capture efficiency of HONO in the biomass combustion environment, which assures the accuracy of the isotopic composition analysis and applicability of this method for field-based biomass combustion research.

3.3 Isotopic composition of HONO and NO_x from burning different biomass

$\delta^{15}N$ of NO_x and HONO emitted from burning various biomass types in this study ranged from -4.3 ‰ to +7.0‰ and -5.3 to +5.8‰, respectively (Table 1). There is no direct dependence of $\delta^{15}N$ on concentration of either HONO or NO_x (Figure S2). In Fig. 4, $\delta^{15}N$ values of NO_x and HONO are shown for each biomass type. Each value represents a concentration-weighted mean (if multiple samples were collected for a biomass type) with error bars representing propagation of replicate variation and method precision. For biomass types burned in replicate (ponderosa pine, lodgepole pine, Engelmann spruce, and Douglas-fir), the $\delta^{15}N$-NO_x and $\delta^{15}N$-HONO variation within a given biomass type is smaller than the full range across all fuel types. Additionally, we note that the variations of $\delta^{15}N$-NO_x and $\delta^{15}N$-HONO for ponderosa pine and $\delta^{15}N$-HONO for Engelmann spruce are larger than the method analytical precision of $\delta^{15}N$-NO_x (1.5‰) and $\delta^{15}N$-HONO (0.5‰), respectively, which represents fire-by-fire variation likely due to different combustion conditions and/or different fuel compositions. For example, fuel moisture content derived from the original biomass weight and dry biomass weight reveal that the ponderosa pine burned in fire no.3 had more moisture content (48.1%) than fire no.2 (32.1%), which could affect combustion temperature and thus product formation. Fig. 4 also illustrates burning different biomass parts from specific vegetation can result in fairly diverse $\delta^{15}N$-HONO and $\delta^{15}N$-NO_x, e.g. among ponderosa pine mixture, canopy and litter, as well as between Engelmann spruce mixture and duff.

Our $\delta^{15}N$-NO_x range falls well within the range (-7‰ to +12‰) found in the FLAME-4 experiment (Fibiger and Hastings, 2016). The FLAME-4 study investigated NO_x emissions from burning a relatively large range of vegetation biomass from all over the world, and found a linear relationship (Eq. (5)), indicating that 83% of the variation of $\delta^{15}N$-NO_x is explained by $\delta^{15}N$-biomass. The biomass types burned in this work focused on vegetation in the western U.S., and differ greatly from that in FLAME-4, with Ponderosa pine being the only common biomass between the two studies. Specifically, the $\delta^{15}N$-biomass range (-4.2‰ to +0.9‰) for this work is much narrower than that of the FLAME-4 experiment (-8‰ to +8‰).

$$\delta^{15}N\text{-}NO_x = 0.41\ \delta^{15}N\text{-biomass} + 1.0\ (r^2=0.83,\ p<0.001) \qquad \text{Eq. (5)}$$

To compare with the relationship found in Fibiger and Hastings (2016) we mass weighted the contributions from different components of the same biomass type. For the same type

of biomass, δ^{15}N-biomass varies amongst different parts of the vegetation with differences as great as 4.1‰, 2.4‰, 4.6‰ and 2.6‰ for ponderosa pine, lodgepole pine, Douglas-fir and Engelmann spruce, respectively (Table S1). In the FIREX experiments, many of the burns were conducted for mixtures of various vegetation parts. For instance, one ponderosa pine fire contains canopy (~30%), litter (~28%), and other parts (~42%) including duff and shrub, and the compositions vary slightly amongst each burn. Therefore, the δ^{15}N of a particular biomass mixture is mass weighted according to its composition contribution from each part (Table S1). Similarly, the δ^{15}N-NO_x and δ^{15}N-HONO from fires of different biomass parts are weighted by concentrations for each biomass type, i.e. ponderosa pine (including mixture, canopy and litter) and Engelmann spruce (including mixture and duff), to produce a signature associated with combustion of that biomass type.

For purpose of comparison among different biomass types, we average δ^{15}N-NO_x (δ^{15}N-HONO) weighted by concentrations for each biomass type, i.e. ponderosa pine (including mixture, canopy and litter) and Engelmann spruce (including mixture and duff) (all data are listed in Table S3). Linear regressions between δ^{15}N-HONO and δ^{15}N-biomass, as well as that between δ^{15}N-NO_x and δ^{15}N-biomass, show that both δ^{15}N-HONO and δ^{15}N-NO_x increase with δ^{15}N-biomass in general (Fig. S3). However, the linear regressions performed here are limited by small datasets (4 data points each) and unsurprisingly yield insignificant linear correlations for δ^{15}N-HONO (or δ^{15}N-NO_x) versus δ^{15}N-biomass (p values are 0.1 and 0.5, respectively). Still, combining our results of δ^{15}N-NO_x versus δ^{15}N-biomass from this work with those from the FLAME-4 study (Fibiger and Hastings, 2016) results in a significant linear correlation (Eq. (6)) and is shown in Fig. 5. Despite differences in burned biomass types between the two studies, our δ^{15}N-NO_x reasonably overlap with the FLAME-4 results within our δ^{15}N-biomass range. The relationship between δ^{15}N-NO_x and δ^{15}N-biomass (Eq. (6)) for the combined data highly reproduces that obtained solely from FLAME-4 study (Eq. (5)) and confirms the dependence of δ^{15}N-NO_x on δ^{15}N-biomass.

$$\delta^{15}\text{N-NO}_x = (0.42\pm0.17)\ \delta^{15}\text{N-biomass} + 1.3\ (r^2=0.71,\ p<0.001) \qquad \text{Eq. (6)}$$

The mean values weighted by concentration plotted in Fig. 4 show ^{15}N of HONO is consistently slightly more depleted than that of NO_x (δ^{15}N-HONO < δ^{15}N-NO_x) across all the biomass types, except for ponderosa pine (litter) that results in an opposite relationship between δ^{15}N-HONO and δ^{15}N-NO_x. Furthermore, δ^{15}N-HONO is linearly correlated with δ^{15}N-NO_x following a relationship of Eq. (7) within the δ^{15}N-NO_x and δ^{15}N-HONO range obtained in the current study (Fig. 6). This provides potential insights into HONO-NO_x interactions and HONO formation pathways in fresh emissions from biomass burning. Although a number of studies on wildfire biomass burning have suggested that partitioning of N emissions between NO_x and NH_3 depends on combustion conditions represented by MCE (Ferek et al., 1998; Goode et al., 1999; McMeeking et al., 2009; Yokelson et al., 1996, 2008), HONO formation pathways remain unclear (Alvarado et al., 2009, 2015; Nie et al., 2015).

$$\delta^{15}\text{N-HONO} = 1.01\ \delta^{15}\text{N-NO}_x - 1.52\ (R^2 = 0.89,\ p<0.001) \qquad \text{Eq. (7)}$$

Previous mechanistic studies on combustion of biomass/biofuel model compounds in a well controlled closed system have investigated detailed nitrogen chemistry in the gas phase, suggesting NO_x and HONO are formed from chain reactions involving oxidation of precursors NH_3 and HCN, which are produced via devolatilization and pyrolysis of amines and proteins in biomass/biofuel (Houshfar et al., 2012; Lucassen et al., 2011). When the combustion conditions favor the oxidation of NH_3 and HCN, NO is first formed and the chain reactions control the cycling of reactive nitrogen species (NO, NO_2 and HONO). Detailed and mechanistic nitrogen chemistry for the chemical relationship between NO_x and HONO in the combustion environment have been discussed in earlier works (Chai and Goldsmith, 2017; Shrestha et al., 2018; Skreiberg et al., 2004). In addition, Houshfar et al. (2012) performed biomass combustion kinetic modeling with reduced mechanism via sensitivity analysis. From these works, we extract major pathways (R1-R11) that are likely responsible for fast gas-phase inter-conversion between NO_x and HONO within the combustion system. They found that whether HONO is preferably converted from NO or NO_2 in series during nitrogen transformation (referred to as nitrogen flow) critically depends on temperature. Specifically, within 1 second of residence time, at moderate temperatures (e.g. 700 °C), preferable nitrogen flow following NO formation in biomass combustion is NO→NO_2→HONO→NO, and major reactions involving NO_x-HONO conversion are listed in R1-R6; at high temperatures (e.g. 850 °C and above), the nitrogen flow cycle NO→HONO→NO_2→NO becomes preferable, and major reactions involving NO_x-HONO are R7-R11.

$NO_2 + HNOH \rightarrow HONO + HNO$ R1

$NO_2 + HNO \rightarrow HONO + NO$ R2

$NO_2 + HO_2 \rightarrow HONO + O_2$ R3

$NO_2 + H_2 \rightarrow HONO + H$ R4

$NO_2 + C_xH_y$ (hydrocarbon) $\rightarrow HONO + C_xH_{y-1}$ R5

$HONO \rightarrow OH + NO$ R6

$OH + NO \rightarrow HONO$ R7

$HONO + NH_2 \rightarrow NO_2 + NH_3$ R8

$HONO + NH \rightarrow NO_2 + NH_2$ R9

$HONO + O \rightarrow NO_2 + OH$ R10

$HONO + OH \rightarrow NO_2 + H_2O$ R11

Although our studied fuels are more complicated in composition than a model system involving no more than a few starting species, results from the above studies provide fundamental underpinnings for biomass combustion. Also note that heterogeneous chemistry after these species were emitted was not considered here as the residence time

of the fresh plume in our study was ~5 seconds, which is of the same magnitude as that predicted in the nitrogen flow analysis (Houshfar et al., 2012). Kinetic isotope effects (KIE) of these reactions have not been characterized; so only a semi-quantitative prediction is presented here. At low temperatures, R1-R5 are all H-abstraction reactions involving loose transition states that have significant activation energy; a primary KIE is expected for such conditions and leads to ^{15}N depletion in the product (HONO) (Chai et al., 2014; Matsson and Westaway, 1999, and references therein). Additionally, R6 is a unimolecular dissociation reaction with no reaction barrier, and hence R6 could be expected to have a small kinetic isotope effect enriching ^{15}N in HONO, somewhat offsetting the depletion that arose from R1-R5. Consequently, the overall isotope effect of R1-R6 would lead to $\delta^{15}N\text{-HONO} < \delta^{15}N\text{-}NO_x$ by a small difference, consistent with our results (Fig. 4). On the other hand, the KIE for the reactions R7-R11 at higher temperatures (> 850 °C) is expected to enrich ^{15}N in HONO relative to NO_x (Chai and Dibble, 2014), leading to an opposite isotope effect to that predicted at lower temperatures.

Temperatures of the biomass combustion process span a large range involving different processes including preheating, drying, distillation, pyrolysis, gasification (aka "glowing combustion") and oxidation in turbulent diffusion flames at a range of temperatures associated with changing flame dynamics (Yokelson et al., 1996). Despite this complexity, our measured slight ^{15}N enrichment in NO_x compared to HONO (Table 1, Fig. 4) suggests that the reactions R1-R6 played a more important role than R7-R11 in HONO formation during the FIREX Fire Lab experiments.

3.4 Isotopic composition of nitrates collected on particle filters

All Nylasorb filter extract solutions showed no detectable NO_3^- and NO_2^- concentrations, indicating no significant amount of HNO_3 was collected on these filters, which is consistent with the very low concentrations measured by MC/IC (note that low concentration and limited sample volume also preclude further isotopic analysis of HNO_3 collected by MC/IC). By contrast, we found 5 out of 20 particulate filter extract solutions had detectable NO_3^- concentration that were sufficient (10 nmol N) for isotopic composition analysis (Table 1). $\delta^{15}N$ and $\delta^{18}O$ reported here are considered to represent $NO_3^-(p)$. $\delta^{15}N\text{-}NO_3^-(p)$ of the five samples (burns) range from -10.6 to -7.4 ‰, all of which are more ^{15}N depleted than that of HONO and NO_x. In addition, the smaller range of $\delta^{15}N\text{-}NO_3^-$ than that of $\delta^{15}N$-HONO and $\delta^{15}N\text{-}NO_x$ rules out possible transformation of NO_x and HONO to nitrate on the filters, which could distort the isotopic composition of NO_x and HONO.

In the FLAME-4 experiments, only one particulate filter had captured $NO_3^-(p)$ above the concentration detection limit, whereas HNO_3 collected on Nylasorb filters from 7 experiments were above the concentration detection limit and therefore only $\delta^{15}N\text{-}HNO_3$ (-0.3‰ to 11.2‰) were reported (Fibiger and Hastings, 2016). The contrast with our filter results are likely attributed to different formation mechanisms under different conditions, in addition to variation of fuel types. Of the 7 detectable HNO_3 collections from FLAME-4, 5 represented room burns for which samples were collected from smoke aged for 1-2 hours in the lab, and the sampled HNO_3 was likely a secondary product. By

583 contrast all our observed NO_3^-(p) were in fresh emissions and may have been derived
584 from plant nitrate (Cárdenas-Navarro et al., 1999) and/or combustion reactions. There
585 have been no other studies on $\delta^{15}N$ of NO_3^-(p) and HNO_3 directly emitted from fresh
586 plumes to the best of our knowledge, so more investigation using both laboratory work
587 (isotope effect) and kinetic modeling will be needed in order to understand formation
588 mechanisms of HNO_3 and NO_3^-(p) in the biomass combustion process and their
589 respective isotope effects.
590
591 In addition to $\delta^{15}N$, we report $\delta^{18}O$ of HONO and NO_3^-(p) directly emitted from biomass
592 burning plumes with ranges of 5.2‰ to 15.2‰ and 11.5‰ to 14.8‰, respectively. These
593 are the first observations reported for $\delta^{18}O$ of reactive nitrogen species directly emitted
594 from biomass burning and low values are expected for the $\delta^{18}O$, which, in this case, is
595 mainly extracted from that of molecular oxygen ($\delta^{18}O$ = ~23.5‰) (Kroopnick and Craig,
596 1972), biomass/cellulose ($\delta^{18}O$ = 15‰–35‰), and/or biomass contained water ($\delta^{18}O$ =
597 ~ 0‰– 16‰) (Keel et al., 2016). In field studies where photochemistry and O_3 are
598 inevitably involved in the reactive nitrogen cycle in various stages of aged plumes, we
599 expect to see much more elevated $\delta^{18}O$ values of HONO and NO_3^-(p) due to the
600 extremely high value of $\delta^{18}O$-O_3 (~110‰) (Vicars and Savarino, 2014). Therefore, the
601 $\delta^{18}O$ found in the lab is helpful in understanding conditions where photochemistry would
602 not apply (e.g. nighttime fresh smoke) and should be distinguishable from the expected
603 higher $\delta^{18}O$ that would be found in aged smoke and/or daytime fresh smoke.
604
605 **4 Conclusions**
606
607 In this study we applied new methods for characterizing the isotopic composition of
608 reactive nitrogen species including NO_x ($\delta^{15}N$), HONO ($\delta^{15}N$ and $\delta^{18}O$), and NO_3^-(p)
609 ($\delta^{15}N$ and $\delta^{18}O$) emitted directly from biomass burning. We measured fresh (stack)
610 emissions from 20 laboratory fires of different fuels during the 2016 FIREX Fire Lab
611 experiments. NO_x, HONO and HNO_3 emitted in fresh smoke reached their peak in most
612 of our fires within five minutes of ignition of biomass (i.e. when flaming combustion
613 peaked). The HONO mixing ratio was typically ~2 orders of magnitude larger than
614 HNO_3, and HONO/NO_x ratio ranged from 0.13 to 0.53.
615
616 Our HONO collection method (ADS) for isotopic analysis was applied to biomass
617 burning (BB) for the first time. The good agreement for concentration comparison
618 between our method and 4 high time-resolution HONO concentration methods suggests
619 high collection efficiency of HONO from BB emissions, which ensures accurate isotopic
620 compositional analysis. Comparison with concurrent observations and a previous study
621 show that the combination of our HONO and NO_x collection methods are compatible,
622 allowing for simultaneous determination of the isotopic composition of both HONO and
623 NO_x. This provides important potential for investigating the photochemical and non-
624 photochemical relationships between HONO and NO_x in a variety of environments, and
625 especially in BB plumes.
626
627 $\delta^{15}N$-NO_x emitted from burning various Western U.S. biomass types in this study ranged
628 from -4.3 ‰ to +7.0 ‰, falling well within the range found by Fibiger and Hastings

(2016), although the vegetation types were much broader in the earlier study. We report the first δ^{15}N-HONO emitted directly from burning, ranging from -5.3‰ to +5.8‰. δ^{15}N-NO_x and δ^{15}N-HONO range derived from BB can be further compared with that from other sources using the same methods presented here, and provide insights into source signatures for both NO_x and HONO. This study also showed the important capability of determining δ^{18}O-HONO and δ^{18}O-NO_3^-(p) from BB plumes, and we expect δ^{18}O of both HONO and NO_3^-(p) produced under photochemical conditions will be much higher than the lab results due to the important role of O_3 in reactive nitrogen oxidation.

Interestingly, the linear correlation between δ^{15}N-HONO and δ^{15}N-NO_x for the biomass we studied suggests systematic co-production of NO_x and HONO occurs during biomass combustion and both of them are released as primary pollutants in fresh smoke. The relationship between δ^{15}N-HONO and δ^{15}N-NO_x likely reflects that HONO was produced to a larger extent at moderate combustion temperatures (< ~800 °C) than higher temperatures on the basis of a simplified mechanism for flow of reactive nitrogen species. However, we note that this relationship is derived from all measured δ^{15}N-HONO and δ^{15}N-NO_x in fires ranging from smoldering to flaming, so is not necessarily representative of a particular combustion condition. Still, it is likely that a compilation over a range of conditions is more useful for potentially distinguishing HONO sources and formation pathways in the environment since it will always be a challenge to assess exact combustion temperatures. Determining these relationships in real wildfire smoke will be essential for better constraint on NO_x and HONO budgets, and eventually may improve ozone and secondary aerosol predictions for regional air quality.

Data availability. The data from the laboratory tests are available on request from the corresponding authors. Data from the 2016 Missoula Fire lab are available here: https://esrl.noaa.gov/csd/groups/csd7/measurements/2016firex/FireLab/DataDownload/

Supplement.

Author contribution. JC, MH and JD designed this work. JC and DJM conducted the sample collections at the Fire Lab, with additional support from MH, JD and ES. JC carried out the isotopic composition measurements; DJM supported the isotopic research and interpretation. ES helped analyze the MC/IC data. VS and RY provided the OP-FTIR data. KJZ and SSB provided the ACES data. ARK and CW provided the PTR-ToF data. JC wrote the manuscript, and all authors provided edits and feedback.

Competing interests. The authors declare that they have no conflicts of interest.

Acknowledgement. This work was supported by funding from the National Oceanic and Atmospheric Administration (AC4 Award NA16OAR4310098 to MH) and the National Science Foundation (AGS-1351932 to MH). The FIREX Fire Lab study was supported in part by the NOAA Climate Office's Atmospheric Chemistry, Carbon Cycle, and Climate program. We are grateful for Ruby Ho for laboratory support and Marshall Otter for the biomass δ^{15}N analysis. We also thank James Roberts and Matthew Coggon

for helpful discussions. We are thankful for the two anonymous reviewers for their helpful comments.

References

Akagi, S. K., Craven, J. S., Taylor, J. W., McMeeking, G. R., Yokelson, R. J., Burling, I. R., Urbanski, S. P., Wold, C. E., Seinfeld, J. H., Coe, H., Alvarado, M. J. and Weise, D. R.: Evolution of trace gases and particles emitted by a chaparral fire in California, Atmos Chem Phys, 12(3), 1397–1421, doi:10.5194/acp-12-1397-2012, 2012.

Akagi, S. K., Yokelson, R. J., Burling, I. R., Meinardi, S., Simpson, I., Blake, D. R., McMeeking, G. R., Sullivan, A., Lee, T., Kreidenweis, S., Urbanski, S., Reardon, J., Griffith, D. W. T., Johnson, T. J. and Weise, D. R.: Measurements of reactive trace gases and variable O3 formation rates in some South Carolina biomass burning plumes, Atmos Chem Phys, 13(3), 1141–1165, doi:10.5194/acp-13-1141-2013, 2013.

Alvarado, M. J. and Prinn, R. G.: Formation of ozone and growth of aerosols in young smoke plumes from biomass burning: 1. Lagrangian parcel studies, J. Geophys. Res. Atmospheres, 114(D9), doi:10.1029/2008JD011144, 2009.

Alvarado, M. J., Wang, C. and Prinn, R. G.: Formation of ozone and growth of aerosols in young smoke plumes from biomass burning: 2. Three-dimensional Eulerian studies, J. Geophys. Res. Atmospheres, 114(D9), doi:10.1029/2008JD011186, 2009.

Alvarado, M. J., Lonsdale, C. R., Yokelson, R. J., Akagi, S. K., Coe, H., Craven, J. S., Fischer, E. V., McMeeking, G. R., Seinfeld, J. H., Soni, T., Taylor, J. W., Weise, D. R. and Wold, C. E.: Investigating the links between ozone and organic aerosol chemistry in a biomass burning plume from a prescribed fire in California chaparral, Atmos Chem Phys, 15(12), 6667–6688, doi:10.5194/acp-15-6667-2015, 2015.

Böhlke, J. K., Mroczkowski, S. J. and Coplen, T. B.: Oxygen isotopes in nitrate: new reference materials for 18O:17O:16O measurements and observations on nitrate-water equilibration, Rapid Commun. Mass Spectrom., 17(16), 1835–1846, doi:10.1002/rcm.1123, 2003.

Burling, I. R., Yokelson, R. J., Griffith, D. W. T., Johnson, T. J., Veres, P., Roberts, J. M., Warneke, C., Urbanski, S. P., Reardon, J., Weise, D. R., Hao, W. M. and de Gouw, J.: Laboratory measurements of trace gas emissions from biomass burning of fuel types from the southeastern and southwestern United States, Atmos Chem Phys, 10(22), 11115–11130, doi:10.5194/acp-10-11115-2010, 2010.

Burling, I. R., Yokelson, R. J., Akagi, S. K., Urbanski, S. P., Wold, C. E., Griffith, D. W. T., Johnson, T. J., Reardon, J. and Weise, D. R.: Airborne and ground-based measurements of the trace gases and particles emitted by prescribed fires in the United States, Atmos Chem Phys, 11(23), 12197–12216, doi:10.5194/acp-11-12197-2011, 2011.

709 Cárdenas-Navarro, R., Adamowicz, S. and Robin, P.: Nitrate accumulation in plants: a
710 role for water, J. Exp. Bot., 50(334), 613–624, doi:10.1093/jxb/50.334.613, 1999.

711 Casciotti, K. L., Sigman, D. M., Hastings, M. G., Böhlke, J. K. and Hilkert, A.:
712 Measurement of the Oxygen Isotopic Composition of Nitrate in Seawater and Freshwater
713 Using the Denitrifier Method, Anal. Chem., 74(19), 4905–4912, doi:10.1021/ac020113w,
714 2002.

715 Casciotti, K. L., Böhlke, J. K., McIlvin, M. R., Mroczkowski, S. J. and Hannon, J. E.:
716 Oxygen Isotopes in Nitrite: Analysis, Calibration, and Equilibration, Anal. Chem., 79(6),
717 2427–2436, doi:10.1021/ac061598h, 2007.

718 Chai, J. and Dibble, T. S.: Pressure Dependence and Kinetic Isotope Effects in the
719 Absolute Rate Constant for Methoxy Radical Reacting with NO2, Int. J. Chem. Kinet.,
720 46(9), 501–511, doi:10.1002/kin.20865, 2014.

721 Chai, J. and Goldsmith, C. F.: Rate coefficients for fuel + NO2: Predictive kinetics for
722 HONO and HNO2 formation, Proc. Combust. Inst., 36(1), 617–626,
723 doi:10.1016/j.proci.2016.06.133, 2017.

724 Chai, J. and Hastings, M.: Collection Method for Isotopic Analysis of Gaseous Nitrous
725 Acid, Anal. Chem., 90(1), 830–838, doi:10.1021/acs.analchem.7b03561, 2018.

726 Chai, J., Hu, H., Dibble, T. S., Tyndall, G. S. and Orlando, J. J.: Rate Constants and
727 Kinetic Isotope Effects for Methoxy Radical Reacting with NO2 and O2, J. Phys. Chem.
728 A, 118(20), 3552–3563 [online] Available from:
729 http://pubs.acs.org/doi/abs/10.1021/jp501205d (Accessed 24 June 2015), 2014.

730 Christian, T. J., Kleiss, B., Yokelson, R. J., Holzinger, R., Crutzen, P. J., Hao, W. M.,
731 Shirai, T. and Blake, D. R.: Comprehensive laboratory measurements of biomass-burning
732 emissions: 2. First intercomparison of open-path FTIR, PTR-MS, and GC-MS/FID/ECD,
733 J. Geophys. Res. Atmospheres, 109(D2), doi:10.1029/2003JD003874, 2004.

734 Cook, P. A., Savage, N. H., Turquety, S., Carver, G. D., O'Connor, F. M., Heckel, A.,
735 Stewart, D., Whalley, L. K., Parker, A. E., Schlager, H., Singh, H. B., Avery, M. A.,
736 Sachse, G. W., Brune, W., Richter, A., Burrows, J. P., Purvis, R., Lewis, A. C., Reeves,
737 C. E., Monks, P. S., Levine, J. G. and Pyle, J. A.: Forest fire plumes over the North
738 Atlantic: p-TOMCAT model simulations with aircraft and satellite measurements from
739 the ITOP/ICARTT campaign, J. Geophys. Res. Atmospheres, 112, D10S43,
740 doi:10.1029/2006JD007563, 2007.

741 Crutzen, P. J. and Andreae, M. O.: Biomass burning in the tropics: impact on atmospheric
742 chemistry and biogeochemical cycles, Science, 250(4988), 1669–1678,
743 doi:10.1126/science.250.4988.1669, 1990.

744 Dibb, J. E., Arsenault, M., Peterson, M. C. and Honrath, R. E.: Fast nitrogen oxide
745 photochemistry in Summit, Greenland snow, Atmos. Environ., 36(15–16), 2501–2511,
746 doi:10.1016/S1352-2310(02)00130-9, 2002.

747 Ferek, R., Reid, J., Hobbs, P., Blake, D. and Liousse, C.: Emission factors of
748 hydrocarbons, halocarbons, trace gases and particles from biomass burning in Brazil, J.
749 Geophys. Res.-ATMOSPHERES, 103, 32107–32118, doi:10.1029/98JD00692, 1998.

750 Fibiger, D. L. and Hastings, M. G.: First Measurements of the Nitrogen Isotopic
751 Composition of NOx from Biomass Burning, Environ. Sci. Technol., 50(21), 11569–
752 11574, doi:10.1021/acs.est.6b03510, 2016.

753 Fibiger, D. L., Hastings, M. G., Lew, A. F. and Peltier, R. E.: Collection of NO and NO2
754 for Isotopic Analysis of NOx Emissions, Anal. Chem., 86(24), 12115–12121,
755 doi:10.1021/ac502968e, 2014.

756 FIREX: FIREX 2016 Fire Lab Data Archive, [online] Available from:
757 https://esrl.noaa.gov/csd/groups/csd7/measurements/2016firex/FireLab/DataDownload/in
758 dex.php?page=/csd/groups/csd7/measurements/2016firex/FireLab/DataDownload/
759 (Accessed 25 March 2019), 2016.

760 Goode, J. G., Yokelson, R. J., Susott, R. A. and Ward, D. E.: Trace gas emissions from
761 laboratory biomass fires measured by open-path Fourier transform infrared spectroscopy:
762 Fires in grass and surface fuels, J. Geophys. Res., 104, 21, doi:10.1029/1999JD900360,
763 1999.

764 Hastings, M. G., Casciotti, K. L. and Elliott, E. M.: Stable Isotopes as Tracers of
765 Anthropogenic Nitrogen Sources, Deposition, and Impacts, Elements, 9(5), 339–344,
766 doi:10.2113/gselements.9.5.339, 2013.

767 Houshfar, E., Skreiberg, Ø., Glarborg, P. and Løvås, T.: Reduced chemical kinetic
768 mechanisms for NO_x emission prediction in biomass combustion, Int. J. Chem. Kinet.,
769 4(44), 219–231, doi:10.1002/kin.20716, 2012.

770 Jaeglé, L., Steinberger, L., Martin, R. V. and Chance, K.: Global partitioning of NOx
771 sources using satellite observations: relative roles of fossil fuel combustion, biomass
772 burning and soil emissions, Faraday Discuss., 130, 407–423; discussion 491-517, 519–
773 524, 2005.

774 Jaffe, D. and Briggs, N.: Ozone production from wildfires: A critical review, Atmos.
775 Environ., 51, 1–10, doi:10.1016/j.atmosenv.2011.11.063, 2012.

776 Keel, S. G., Joos, F., Spahni, R., Saurer, M., Weigt, R. B. and Klesse, S.: Simulating
777 oxygen isotope ratios in tree ring cellulose using a dynamic global vegetation model,
778 Biogeosciences, 13(13), 3869–3886, doi:https://doi.org/10.5194/bg-13-3869-2016, 2016.

779 Keene, W. C., Lobert, J. M., Crutzen, P. J., Maben, J. R., Scharffe, D. H., Landmann, T.,
780 Hély, C. and Brain, C.: Emissions of major gaseous and particulate species during
781 experimental burns of southern African biomass, J. Geophys. Res. Atmospheres,
782 111(D4), doi:10.1029/2005JD006319, 2006.

783 Koss, A. R., Sekimoto, K., Gilman, J. B., Selimovic, V., Coggon, M. M., Zarzana, K. J.,
784 Yuan, B., Lerner, B. M., Brown, S. S., Jimenez, J. L., Krechmer, J., Roberts, J. M.,
785 Warneke, C., Yokelson, R. J. and Gouw, J. de: Non-methane organic gas emissions from
786 biomass burning: identification, quantification, and emission factors from PTR-ToF
787 during the FIREX 2016 laboratory experiment, Atmospheric Chem. Phys., 18(5), 3299–
788 3319, doi:https://doi.org/10.5194/acp-18-3299-2018, 2018.

789 Kraus, S.: DOASIS: a framework design for DOAS., 2006.

790 Kroopnick, P. and Craig, H.: Atmospheric oxygen: isotopic composition and solubility
791 fractionation, Science, 175(4017), 54–55, doi:10.1126/science.175.4017.54, 1972.

792 Lapina, K., Honrath R. E., Owen R. C., Val Martín M., Hyer E. J. and Fialho P.: Late
793 summer changes in burning conditions in the boreal regions and their implications for
794 NOx and CO emissions from boreal fires, J. Geophys. Res. Atmospheres, 113(D11),
795 doi:10.1029/2007JD009421, 2008.

796 Liu, X., Zhang, Y., Huey, L. G., Yokelson, R. J., Wang, Y., Jimenez, J. L., Campuzano-
797 Jost, P., Beyersdorf, A. J., Blake, D. R., Choi, Y., Clair, J. M. S., Crounse, J. D., Day, D.
798 A., Diskin, G. S., Fried, A., Hall, S. R., Hanisco, T. F., King, L. E., Meinardi, S.,
799 Mikoviny, T., Palm, B. B., Peischl, J., Perring, A. E., Pollack, I. B., Ryerson, T. B.,
800 Sachse, G., Schwarz, J. P., Simpson, I. J., Tanner, D. J., Thornhill, K. L., Ullmann, K.,
801 Weber, R. J., Wennberg, P. O., Wisthaler, A., Wolfe, G. M. and Ziemba, L. D.:
802 Agricultural fires in the southeastern U.S. during SEAC4RS: Emissions of trace gases
803 and particles and evolution of ozone, reactive nitrogen, and organic aerosol, J. Geophys.
804 Res. Atmospheres, 121(12), 7383–7414, doi:10.1002/2016JD025040, 2016.

805 Lucassen, A., Labbe, N., Westmoreland, P. R. and Kohse-Höinghaus, K.: Combustion
806 chemistry and fuel-nitrogen conversion in a laminar premixed flame of morpholine as a
807 model biofuel, Combust. Flame, 158(9), 1647–1666,
808 doi:10.1016/j.combustflame.2011.02.010, 2011.

809 Matsson, O. and Westaway, K. C.: Secondary Deuterium Kinetic Isotope Effects and
810 Transition State Structure, in Advances in Physical Organic Chemistry, vol. 31, edited by
811 D. Bethell, pp. 143–248, Academic Press., 1999.

812 McMeeking, G. R., Kreidenweis, S. M., Baker, S., Carrico, C. M., Chow, J. C., Collett, J.
813 L., Hao, W. M., Holden, A. S., Kirchstetter, T. W., Malm, W. C., Moosmüller, H.,
814 Sullivan, A. P. and Wold, C. E.: Emissions of trace gases and aerosols during the open
815 combustion of biomass in the laboratory, J. Geophys. Res. Atmospheres, 114(D19),
816 D19210, doi:10.1029/2009JD011836, 2009.

817 Miller, D. J., Wojtal, P. K., Clark, S. C. and Hastings, M. G.: Vehicle NOx emission
818 plume isotopic signatures: Spatial variability across the eastern United States, J. Geophys.
819 Res. Atmospheres, 122(8), 4698–4717, doi:10.1002/2016JD025877, 2017.

820 Miller, D. J., Chai, J., Guo, F., Dell, C. J., Karsten, H. and Hastings, M. G.: Isotopic
821 Composition of In Situ Soil NOx Emissions in Manure-Fertilized Cropland, Geophys.
822 Res. Lett., 45(21), 12,058-12,066, doi:10.1029/2018GL079619, 2018.

823 Min, K.-E., Washenfelder, R. A., Dubé, W. P., Langford, A. O., Edwards, P. M.,
824 Zarzana, K. J., Stutz, J., Lu, K., Rohrer, F., Zhang, Y. and Brown, S. S.: A broadband
825 cavity enhanced absorption spectrometer for aircraft measurements of glyoxal,
826 methylglyoxal, nitrous acid, nitrogen dioxide, and water vapor, Atmospheric Meas.
827 Tech., 9(2), 423–440, doi:https://doi.org/10.5194/amt-9-423-2016, 2016.

828 Neuman, J. A., Trainer, M., Brown, S. S., Min, K.-E., Nowak, J. B., Parrish, D. D.,
829 Peischl, J., Pollack, I. B., Roberts, J. M., Ryerson, T. B. and Veres, P. R.: HONO
830 emission and production determined from airborne measurements over the Southeast
831 U.S., J. Geophys. Res. Atmospheres, 121(15), 9237–9250, doi:10.1002/2016JD025197,
832 2016.

833 Nie, W., Ding, A. J., Xie, Y. N., Xu, Z., Mao, H., Kerminen, V.-M., Zheng, L. F., Qi, X.
834 M., Huang, X., Yang, X.-Q., Sun, J. N., Herrmann, E., Petäjä, T., Kulmala, M. and Fu, C.
835 B.: Influence of biomass burning plumes on HONO chemistry in eastern China, Atmos
836 Chem Phys, 15(3), 1147–1159, doi:10.5194/acp-15-1147-2015, 2015.

837 Perrino, C., De Santis, F. and Febo, A.: Criteria for the choice of a denuder sampling
838 technique devoted to the measurement of atmospheric nirous and nitric acids,
839 Atmospheric Environ. Part Gen. Top., 24(3), 617–626, doi:10.1016/0960-
840 1686(90)90017-H, 1990.

841 Pinto, J. P., Dibb, J., Lee, B. H., Rappenglück, B., Wood, E. C., Levy, M., Zhang, R.-Y.,
842 Lefer, B., Ren, X.-R., Stutz, J., Tsai, C., Ackermann, L., Golovko, J., Herndon, S. C.,
843 Oakes, M., Meng, Q.-Y., Munger, J. W., Zahniser, M. and Zheng, J.: Intercomparison of
844 field measurements of nitrous acid (HONO) during the SHARP campaign, J. Geophys.
845 Res. Atmospheres, 119(9), 5583–5601, doi:10.1002/2013JD020287, 2014.

846 Reinhardt, E. D., Keane, R. E. and Brown, J. K.: First Order Fire Effects Model: FOFEM
847 4.0, user's guide, Gen Tech Rep INT-GTR-344 Ogden UT US Dep. Agric. For. Serv.
848 Intermt. Res. Stn. 65 P, 344, doi:10.2737/INT-GTR-344, 1997.

849 Roberts, J. M., Veres, P., Warneke, C., Neuman, J. A., Washenfelder, R. A., Brown, S.
850 S., Baasandorj, M., Burkholder, J. B., Burling, I. R., Johnson, T. J., Yokelson, R. J. and
851 de Gouw, J.: Measurement of HONO, HNCO, and other inorganic acids by negative-ion
852 proton-transfer chemical-ionization mass spectrometry (NI-PT-CIMS): application to
853 biomass burning emissions, Atmos Meas Tech, 3(4), 981–990, doi:10.5194/amt-3-981-
854 2010, 2010.

855 Scheuer, E., Talbot, R. W., Dibb, J. E., Seid, G. K., DeBell, L. and Lefer, B.: Seasonal
856 distributions of fine aerosol sulfate in the North American Arctic basin during TOPSE, J.
857 Geophys. Res. Atmospheres, 108(D4), doi:10.1029/2001JD001364, 2003.

858 Selimovic, V., Yokelson, R. J., Warneke, C., Roberts, J. M., de Gouw, J., Reardon, J. and
859 Griffith, D. W. T.: Aerosol optical properties and trace gas emissions by PAX and OP-
860 FTIR for laboratory-simulated western US wildfires during FIREX, Atmos Chem Phys,
861 18(4), 2929–2948, doi:10.5194/acp-18-2929-2018, 2018.

862 Shrestha, K. P., Seidel, L., Zeuch, T. and Mauss, F.: Detailed Kinetic Mechanism for the
863 Oxidation of Ammonia Including the Formation and Reduction of Nitrogen Oxides,
864 Energy Fuels, doi:10.1021/acs.energyfuels.8b01056, 2018.

865 Sigman, D. M., Casciotti, K. L., Andreani, M., Barford, C., Galanter, M. and Böhlke, J.
866 K.: A Bacterial Method for the Nitrogen Isotopic Analysis of Nitrate in Seawater and
867 Freshwater, Anal. Chem., 73(17), 4145–4153, doi:10.1021/ac010088e, 2001.

868 Skreiberg, Ø., Kilpinen, P. and Glarborg, P.: Ammonia chemistry below 1400 K under
869 fuel-rich conditions in a flow reactor, Combust. Flame, 136(4), 501–518,
870 doi:10.1016/j.combustflame.2003.12.008, 2004.

871 Stockwell, C. E., Yokelson, R. J., Kreidenweis, S. M., Robinson, A. L., DeMott, P. J.,
872 Sullivan, R. C., Reardon, J., Ryan, K. C., Griffith, D. W. T. and Stevens, L.: Trace gas
873 emissions from combustion of peat, crop residue, domestic biofuels, grasses, and other
874 fuels: configuration and Fourier transform infrared (FTIR) component of the fourth Fire
875 Lab at Missoula Experiment (FLAME-4), Atmos Chem Phys, 14(18), 9727–9754,
876 doi:10.5194/acp-14-9727-2014, 2014.

877 Stutz, J., Oh, H.-J., Whitlow, S. I., Anderson, C., Dibb, J. E., Flynn, J. H., Rappenglück,
878 B. and Lefer, B.: Simultaneous DOAS and mist-chamber IC measurements of HONO in
879 Houston, TX, Atmos. Environ., 44(33), 4090–4098, doi:10.1016/j.atmosenv.2009.02.003,
880 2010.

881 Tkacik, D. S., Robinson, E. S., Ahern, A., Saleh, R., Stockwell, C., Veres, P., Simpson, I.
882 J., Meinardi, S., Blake, D. R., Yokelson, R. J., Presto, A. A., Sullivan, R. C., Donahue, N.
883 M. and Robinson, A. L.: A dual-chamber method for quantifying the effects of
884 atmospheric perturbations on secondary organic aerosol formation from biomass burning
885 emissions, J. Geophys. Res. Atmospheres, 122(11), 6043–6058,
886 doi:10.1002/2016JD025784, 2017.

887 Travis, K. R., Jacob, D. J., Fisher, J. A., Kim, P. S., Marais, E. A., Zhu, L., Yu, K.,
888 Miller, C. C., Yantosca, R. M., Sulprizio, M. P., Thompson, A. M., Wennberg, P. O.,
889 Crounse, J. D., St. Clair, J. M., Cohen, R. C., Laughner, J. L., Dibb, J. E., Hall, S. R.,
890 Ullmann, K., Wolfe, G. M., Pollack, I. B., Peischl, J., Neuman, J. A. and Zhou, X.: Why
891 do models overestimate surface ozone in the Southeast United States?, Atmos Chem
892 Phys, 16(21), 13561–13577, doi:10.5194/acp-16-13561-2016, 2016.

893 Trentmann, J., Yokelson, R. J., Hobbs, P. V., Winterrath, T., Christian, T. J., Andreae, M.
894 O. and Mason, S. A.: An analysis of the chemical processes in the smoke plume from a
895 savanna fire, J. Geophys. Res. Atmospheres, 110(D12), doi:10.1029/2004JD005628,
896 2005.

Val Martín, M., Honrath, R. E., Owen, R. C., Pfister, G., Fialho, P. and Barata, F.: Significant enhancements of nitrogen oxides, black carbon, and ozone in the North Atlantic lower free troposphere resulting from North American boreal wildfires, J. Geophys. Res. Atmospheres, 111(D23), doi:10.1029/2006JD007530, 2006.

Veres, P., Roberts, J. M., Burling, I. R., Warneke, C., Gouw, J. de and Yokelson, R. J.: Measurements of gas-phase inorganic and organic acids from biomass fires by negative-ion proton-transfer chemical-ionization mass spectrometry, J. Geophys. Res. Atmospheres, 115(D23), doi:10.1029/2010JD014033, 2010.

Vicars, W. C. and Savarino, J.: Quantitative constraints on the 17O-excess (Δ17O) signature of surface ozone: Ambient measurements from 50°N to 50°S using the nitrite-coated filter technique, Geochim. Cosmochim. Acta, 135(Supplement C), 270–287, doi:10.1016/j.gca.2014.03.023, 2014.

Wojtal, P. K., Miller, D. J., O'Conner, M., Clark, S. C. and Hastings, M. G.: Automated, High-resolution Mobile Collection System for the Nitrogen Isotopic Analysis of NOx, J. Vis. Exp. JoVE, (118), doi:10.3791/54962, 2016.

Ye, C., Zhou, X., Pu, D., Stutz, J., Festa, J., Spolaor, M., Tsai, C., Cantrell, C., Mauldin, R. L., Campos, T., Weinheimer, A., Hornbrook, R. S., Apel, E. C., Guenther, A., Kaser, L., Yuan, B., Karl, T., Haggerty, J., Hall, S., Ullmann, K., Smith, J. N., Ortega, J. and Knote, C.: Rapid cycling of reactive nitrogen in the marine boundary layer, Nature, 532(7600), 489–491, doi:10.1038/nature17195, 2016.

Yokelson, R., W. T. Griffith, D. and Ward, D.: Open-path Fourier transform infrared studies of large-scale laboratory biomass fires, J. Geophys. Res., 101, 21067, doi:10.1029/96JD01800, 1996.

Yokelson, R. J., Karl, T., Artaxo, P., Blake, D. R., Christian, T. J., Griffith, D. W. T., Guenther, A. and Hao, W. M.: The Tropical Forest and Fire Emissions Experiment: overview and airborne fire emission factor measurements, Atmos Chem Phys, 7(19), 5175–5196, doi:10.5194/acp-7-5175-2007, 2007.

Yokelson, R. J., Christian, T. J., Karl, T. G. and Guenther, A.: The tropical forest and fire emissions experiment: laboratory fire measurements and synthesis of campaign data, Atmos Chem Phys, 8(13), 3509–3527, doi:10.5194/acp-8-3509-2008, 2008.

Yokelson, R. J., Crounse, J. D., DeCarlo, P. F., Karl, T., Urbanski, S., Atlas, E., Campos, T., Shinozuka, Y., Kapustin, V., Clarke, A. D., Weinheimer, A., Knapp, D. J., Montzka, D. D., Holloway, J., Weibring, P., Flocke, F., Zheng, W., Toohey, D., Wennberg, P. O., Wiedinmyer, C., Mauldin, L., Fried, A., Richter, D., Walega, J., Jimenez, J. L., Adachi, K., Buseck, P. R., Hall, S. R. and Shetter, R.: Emissions from biomass burning in the Yucatan, Atmos Chem Phys, 9(15), 5785–5812, doi:10.5194/acp-9-5785-2009, 2009.

Yuan, B., Koss, A., Warneke, C., Gilman, J. B., Lerner, B. M., Stark, H. and Gouw, J. A. de: A high-resolution time-of-flight chemical ionization mass spectrometer utilizing hydronium ions (H_3O^+ ToF-CIMS) for measurements of volatile organic compounds in

the atmosphere, Atmospheric Meas. Tech., 9(6), 2735–2752, doi:https://doi.org/10.5194/amt-9-2735-2016, 2016.

Zarzana, K. J., Selimovic, V., Koss, A. R., Sekimoto, K., Coggon, M. M., Yuan, B., Dubé, W. P., Yokelson, R. J., Warneke, C., Gouw, J. A. de, Roberts, J. M. and Brown, S. S.: Primary emissions of glyoxal and methylglyoxal from laboratory measurements of open biomass burning, Atmospheric Chem. Phys., 18(20), 15451–15470, doi:https://doi.org/10.5194/acp-18-15451-2018, 2018.

Zhou, S., Young, C. J., VandenBoer, T. C., Kowal, S. F. and Kahan, T. F.: Time-Resolved Measurements of Nitric Oxide, Nitrogen Dioxide, and Nitrous Acid in an Occupied New York Home, Environ. Sci. Technol., 52(15), 8355–8364, doi:10.1021/acs.est.8b01792, 2018.

Table 1. Concentration (mean, derived from solution concentration and flow rate) and N isotopic composition for various biomass burning experiments, unit for all δ denotations is ‰. MCE values are extracted from NOAA FIREX fire archive. Note: fire no. 1, 7 and 13 were missing due to technical issues; NO_x results are only shown when blank/sample ratio is <70%. Biomass acronyms are defined in Sect. 2.1; in addition, d—duff, c—canopy, l-litter.

Biomass	Fire no.	HONO (ppbv)	$\delta^{15}N$-HONO	$\delta^{18}O$-HONO	NO_x (ppbv)	$\delta^{15}N$-NO_x	$\delta^{15}N$-biomass	$\delta^{15}N$-p-NO_3^-	$\delta^{18}O$-p-NO_3^-	HONO/NO_x	MCE
PIPO	2	19.9	-5.3	12.6	147.9	-1.1	0.3	-7.5	14.3	0.13	0.93
PIPO	3	35.8	1.7	11.6	124.7	2.3	0.3			0.29	0.94
PIPO	4	152.9	-3.1	10.6	716.8	-3.6	0.3			0.21	0.93
PICO	5	74.8	-2.3	8.8	170.8	-1.1	-3.4	-7.4	14.8	0.44	0.93
PICO	6	17.6	-1.9	8.4	94.7	1.4	-3.4			0.19	0.94
PIEN	8	25.7	-1.7	14.6	91.7	0.1	-2.4			0.28	0.92
PIEN	9	21.3	-4.8	9.5	73.6	-1.3	-2.8			0.29	0.93
PSME	10	42.2	-0.5	5.2	229.7	1.9	-1.4	-10.6	14.5	0.18	0.94
PSME	11	112.3	-0.4	15.2	571.8	3.3	-2.0			0.20	0.95
PIEN-d	12	17.1	-4.6	8.5	36.2	-4.3	-1.4	-9.9	11.5	0.47	0.87
PSME	14	25.3	0.1	14.9	70.0	2.1	-1.9			0.36	0.93
ABLA-c	15	51.0	2.1	9.9	95.5	3.4	-2.6	-8.9	12.7	0.53	0.89
PIPO-l	16	70.0	5.8	7.5	443.3	5.2	0.9			0.16	0.95
PIEN-c	17	47.1	6.1	14.8			-3.5				0.89
PSME-c	18	45.3	2.5	14.0			-1.4				0.93
PIPO-c	19	23.8	5.3	14.8	73.3	7.0	-0.1			0.32	0.93
PICO-c	20	52.5	3.0	14.9			-3.1				0.94
PICO-l	21	9.9	0.3	15.2			-4.2				0.93
PSME-l	22	40.0	1.9	10.2			-2.3				0.95
ABLA-c	23	40.8	0.5	12.2			-2.6				0.95

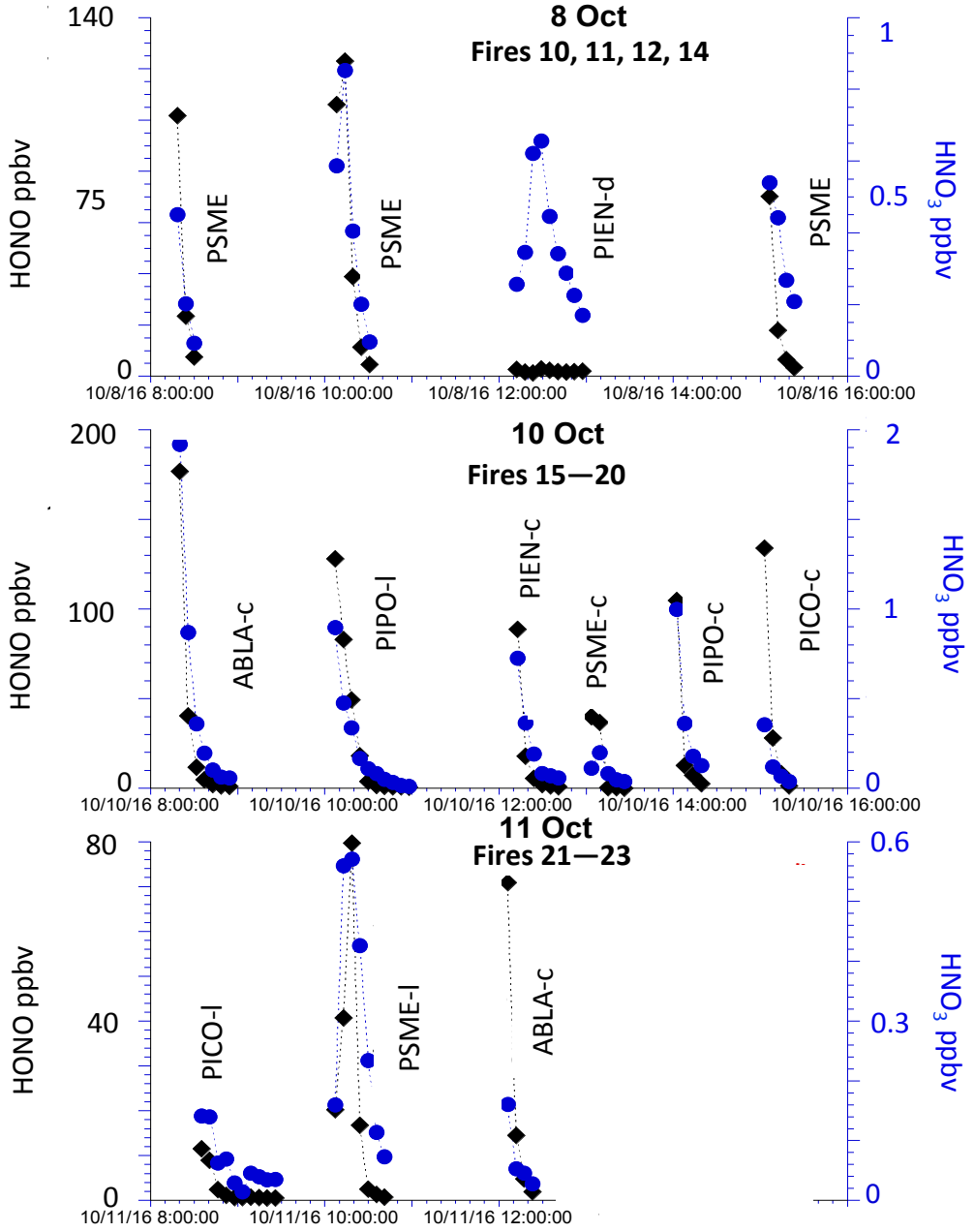

Figure 1. Temporal profile of HONO (black diamond) and HNO_3 (blue circle) concentration measured using MC/IC method for various stack fires (fire numbers are referred to Table 1).

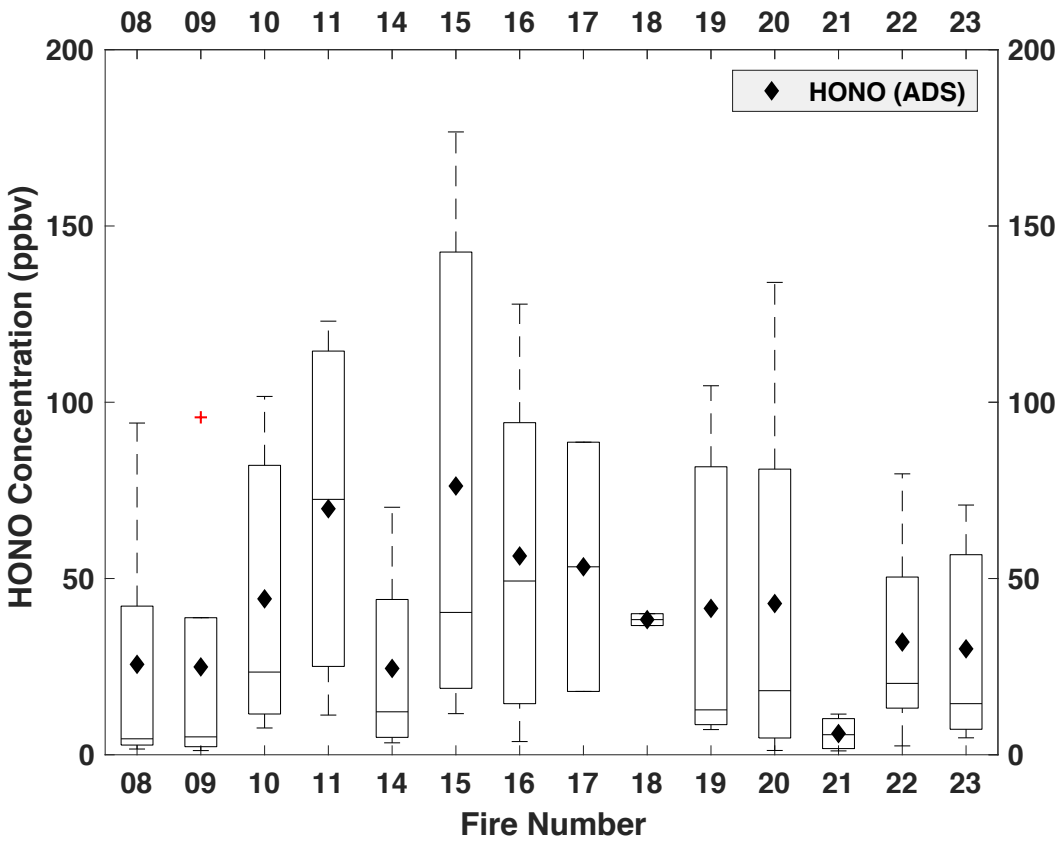

Figure 2. Box plot of MC/IC HONO measurement with 5 minutes resolution over the course of each fire. Each box whisker represents 5th, 25th, 50th, 75th, 95th percentile of HONO concentration during each collection period. Black diamond is the mean HONO concentration recovered from ADS collection. The red cross symbolize outliers. Note no isotopic analysis was performed for fire no. 12 (shown in Figure 1) due to insufficient amount of collected nitrite.

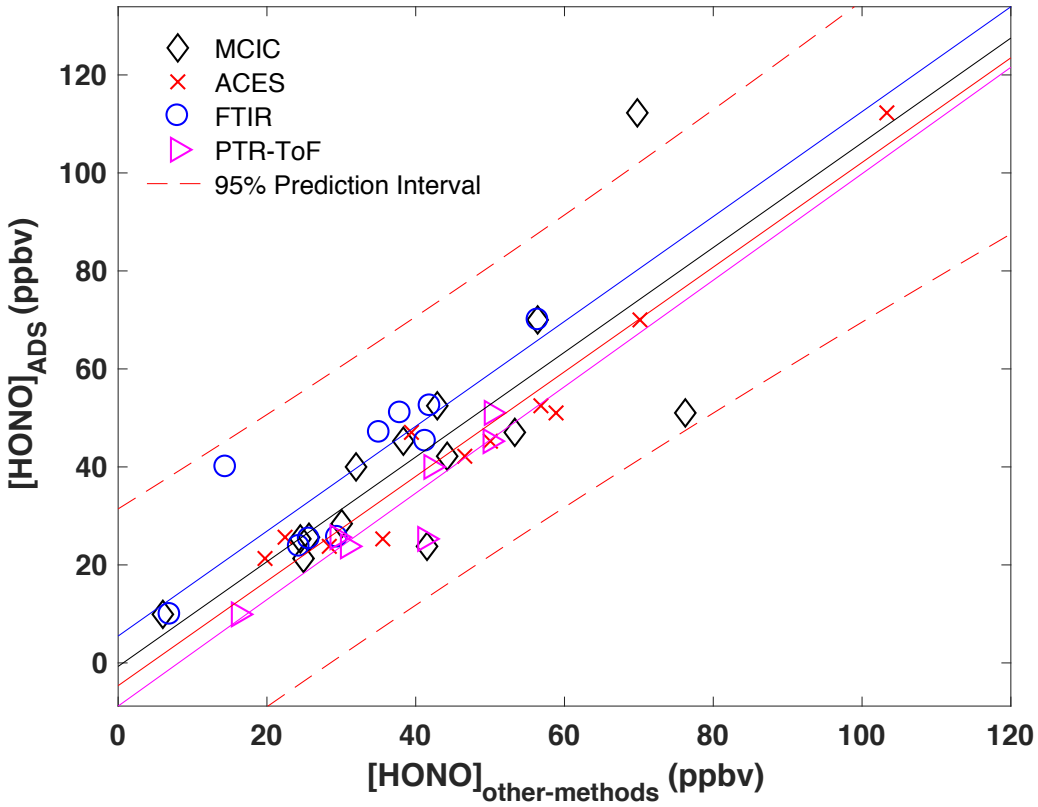

Figure 3. Comparison of ADS measured HONO concentration with mean values of various high resolution methods including MC/IC, FTIR, ACES and PTR-ToF for available fires. Solid lines are linear regression of each dataset with the same symbol color.

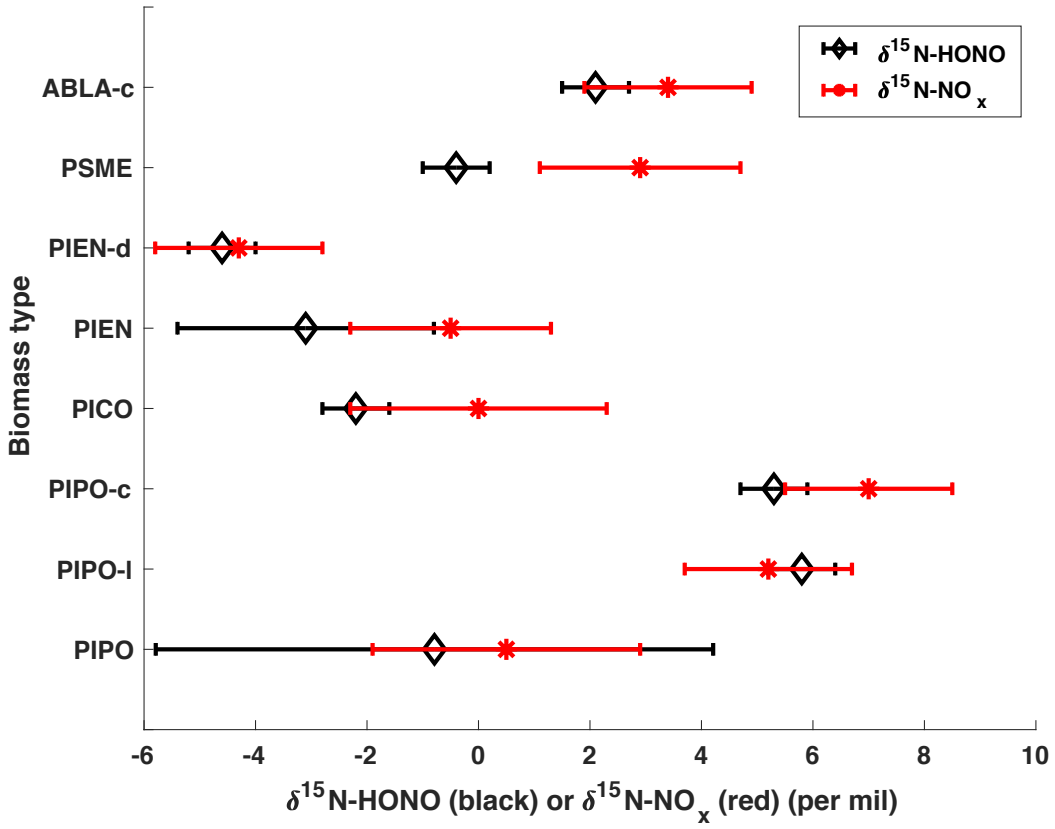

Figure 4. Concentration weighted mean δ^{15}N- of HONO and NO_x versus biomass type. The error bars are propagation of replicate ±1σ uncertainty (when n>1) and method uncertainty; otherwise, the error bars stand for method uncertainty. PIPO is ponderosa pine, PICO is lodgepole pine, PIEN is Engelmann spruce, PSME is Douglas-fir, ABLA is subalpine (from Fish Lake, canopy). l indicates litter, c indicates canopy, d indicates duff.

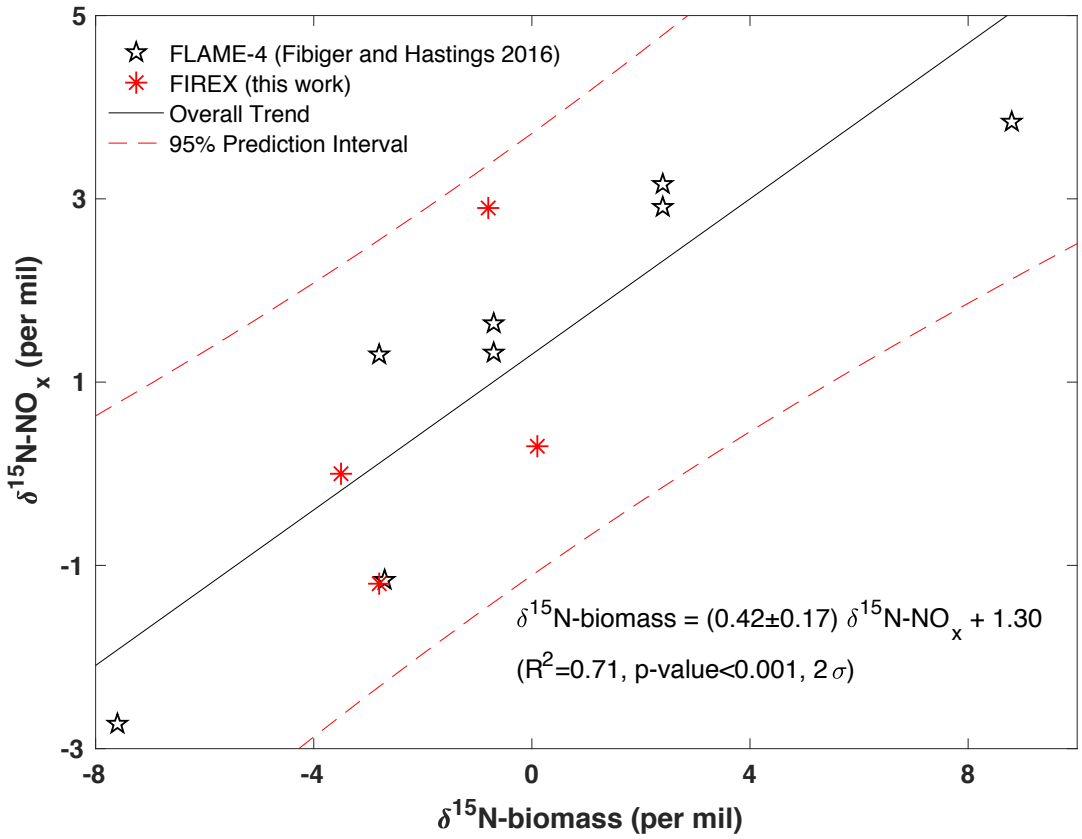

Figure 5. Dependence of δ^{15}N-NO_x on δ^{15}N-biomass. Star data points represent results from FLAME-4 study (Fibiger and Hastings, 2016); Asterisk data points represent results from this work; solid line is linear regression between δ^{15}N-NO_x and δ^{15}N-biomass for the combined dataset; dashed lines are 95% prediction interval (2σ).

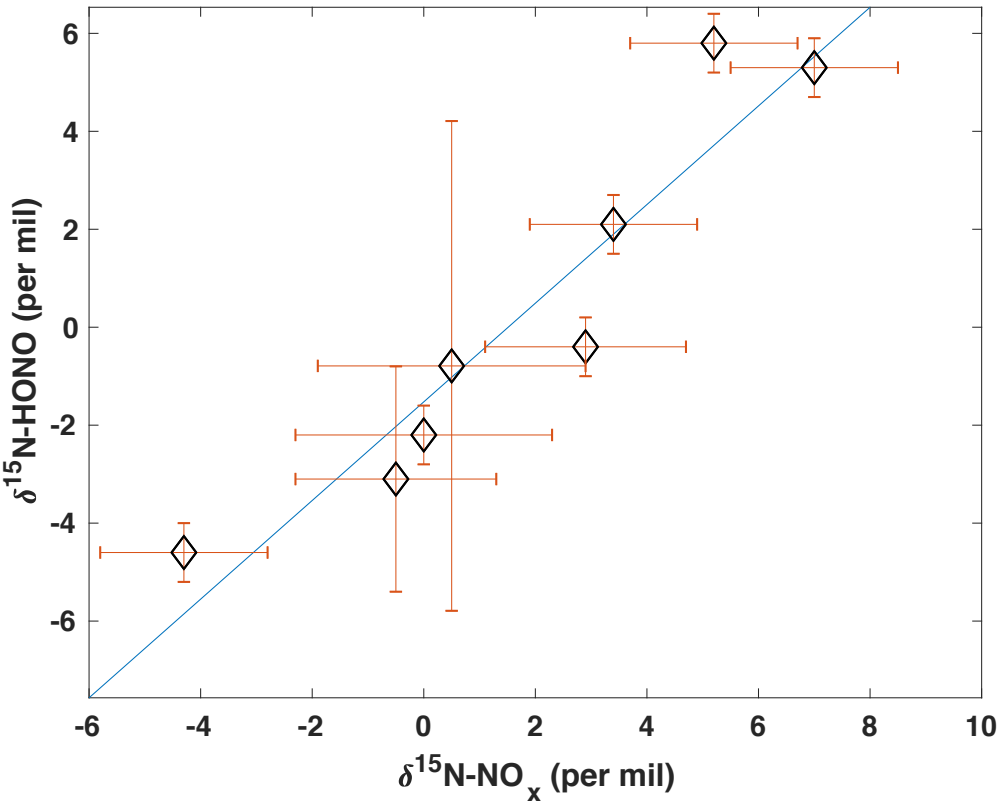

Figure 6. Scatter plot between δ^{15}N-HONO and δ^{15}N-NO_x. All error bars are propagation of replicate uncertainty (±1σ) and method uncertainty. Linear regression follows δ^{15}N-HONO = 1.01 δ^{15}N-NO_x - 1.52 (R^2 = 0.89, p<0.001).

Supplement

Isotopic characterization of nitrogen oxides (NO_x), nitrous acid (HONO), and nitrate (NO_3^-(p)) from laboratory biomass burning during FIREX

Jiajue Chai[1], David J. Miller[1,a], Eric Scheuer[2], Jack Dibb[2], Vanessa Selimovic[3], Robert Yokelson[3], Kyle J. Zarzana[4,5,b], Steven S. Brown[4,6], Abigail R. Koss[4,5,6,c], Carsten Warneke[5,6], Meredith Hastings[1]

1. Department of Earth, Environmental and Planetary Sciences, and Institute at Brown for Environment and Society, Brown University, Providence, RI, USA
2. Institute for the Study of Earth, Ocean and Space, University of New Hampshire, Durham, NH, USA
3. Department of Chemistry, University of Montana, Missoula, USA
4. Chemical Sciences Division, NOAA Earth System Research Laboratory, Boulder, CO, USA
5. Cooperative Institute for Research in Environmental Sciences, University of Colorado, Boulder, CO, USA
6. Department of Chemistry, University of Colorado, Boulder, CO, USA

a. Now at: Environmental Defense Fund, Boston, MA, USA
b. Now at: Department of Chemistry, University of Colorado, Boulder, CO, USA
c. Department of Civil and Environmental Engineering, Massachusetts Institute of Technology, Cambridge, MA, USA

Correspondence: Jiajue Chai (jiajue_chai@brown.edu)

Experimental details

NO_x online concentration measurement

NO and NO_x concentrations were measured with a Thermo Scientific Model 42i chemiluminescence NO/NO_x analyzer, with ±0.4 ppbv precision and 0.2 ppbv zero noise at 1 minute time resolution. In the NO channel, O_3 generated by an ozonator titrates NO to excited state NO_2 which subsequently produces luminescence that is proportional to NO concentration. In the NO_x channel, the sample gas stream first flows through a heated molybdenum catalyst (325 °C) that converts NO_2 to NO before entering the NO+O_3 reaction chamber. The auto cycle mode (NO/NO_x) switches the mode solenoid valve automatically on a 10 second cycle so that NO, NO_2, and NO_x concentrations are determined. It is known that some NO_y species including HONO, HNO_3, organic nitrate and PAN can be partially converted to NO in the hot molybdenum catalyst, causing positive artifacts in measured NO_x (Reed et al., 2016). In this study, only the HONO interference was corrected for. This was done by subtracting the ADS measured HONO concentration (mean value across each whole fire) from Thermo analyzer measured NO_x

concentration averaged across the whole fire; this provided the approximate lower limit of the NO_x concentration by assuming HONO is 100% converted to NO on the Molybdenum catalyst (e.g. (Dunlea et al., 2007; Febo et al., 1995). Contributions from HNO_3, PAN and gaseous organic nitrate are not of major concern because no photo-oxidation is involved in indoor fires (Koss et al., 2018; Selimovic et al., 2018; Stockwell et al., 2014). In addition, we do not expect that other reactive nitrogen species such as NH_3 and hydrogen cyanide (HCN) interfere with NO_2 measurement. A particulate matter filter (Millipore, 1μm PTFE) was always placed before the inlet of the NO_x analyzer. The NO channel was calibrated before and after the entire Fire Lab experiments with standard NO (10 ppmv in N_2) diluted with zero air (Thermo Fisher Scientific, Model 111) via a gas dilution calibrator (Thermo Fisher Scientific, Model 146i) and NO_2 response of the NO_x channel using O_3 titration is within ±5% accuracy. The NO_x measurement verified the concentration of the NO_x collected for isotopic analysis, and the original NO_x data is available in the NOAA FIREX archive (FIREX, 2016).

Table S1 Information of fuels measured for $\delta^{15}N$-biomass. Acronyms: ponderosa pine (PIPO), lodgepole pine (PICO), Engelmann spruce (PIEN), Douglas-fir (PSME) and subalpine fir (ABLA). Each fuel is a mixture of one or multiple compositions (different parts from the vegetation) including duff, litter, canopy, rotten, shrub. $\delta^{15}N$ of each composition (5^{th} column) was measured in replicates using the method described in section 2.2.3. Composition mass weighted $\delta^{15}N$ in 6^{th} column are calculated by mass weighting $\delta^{15}N$ of each composition (5^{th} column) with nitrogen content (=sample weight×%N). Mixture mass weighted $\delta^{15}N$ (8^{th} column) is calculated by mass weighting $\delta^{15}N$ (6^{th} column) with fraction in mixture (7^{th} column).

Sample	Fuel Compo.	Sample Weight (mg)	%N	$\delta^{15}N$ (‰)	Compo. Mass Weighted $\delta^{15}N$ ‰	Fraction in Mixture	Mixture Mass Weighted $\delta^{15}N$ (‰)
PIPO	Duff	4.87	1.11	0.32	0.39	0.16	0.1
PIPO	Duff	5.00	1.11	0.31			
PIPO	Duff	5.36	1.20	0.51			
PIPO	Litter	4.75	0.57	1.27	0.94	0.29	
PIPO	Litter	7.60	0.54	0.59			
PIPO	Canopy	4.76	0.9	-0.11	-0.10	0.31	

			7				
PIPO	Canopy	5.16	0.97	-0.10			
PIPO	Rotten	7.06	0.19	1.15	-1.33	0.18	
PIPO	Rotten	10.14	0.17	-2.29			
PIPO	Rotten	10.30	0.16	-1.55			
PIPO	Rotten	10.37	0.18	-2.82			
PICO	Duff	4.69	0.51	-2.95	-2.53	0.20	-3.5
PICO	Duff	16.31	0.42	-1.83			
PICO	Duff	10.58	0.68	-2.63			
PICO	Litter	4.45	0.84	-2.73	-3.09	0.11	
PICO	Litter	4.75	0.91	-3.38			
PICO	Litter	7.06	0.85	-3.15			
PICO	Canopy	4.45	0.93	-4.17	-4.16	0.40	
PICO	Canopy	5.24	0.88	-4.14			
PICO	Shrub	4.48	0.90	-3.51	-3.36	0.09	
PICO	Shrub	6.60	0.88	-3.21			
PSME	Duff	4.90	0.74	-0.08	0.39	0.15	-0.8
PSME	Duff	9.95	0.87	0.79			
PSME	Litter	4.53	0.72	-2.41	-2.30	0.11	
PSME	Litter	6.69	0.72	-2.19			
PSME	Canopy	4.66	0.87	-2.59	-2.33	0.46	
PSME	Canopy	5.99	0.86	-2.08			
PSME	Rotten	7.76	0.31	2.02	1.67	0.28	
PSME	Rotten	7.08	0.3	1.74			

PSME	Rotten	10.09	1 0.30	1.23			
Chamise	Canopy	5.27	1.14	-3.03	-2.84		
Chamise	Canopy	5.42	1.14	-2.66			
PIEN	Duff	4.68	1.32	-1.38	-1.41	0.17	-2.8
PIEN	Duff	5.03	1.40	-1.43			
PIEN	Canopy	4.59	0.95	-3.95	-3.50	0.31	
PIEN	Canopy	6.19	0.95	-2.70			
PIEN	Canopy	5.48	0.98	-3.84			
ABLA	Duff	5.25	1.17	-1.57	-1.40		
ABLA	Duff	6.47	1.20	-1.25			
ABLA	Litter	4.38	1.00	-4.02	-3.85		
ABLA	Litter	6.24	0.91	-3.66			

Table S2 Comparisons between $[HONO]_{ADS}$ with mean values of various high resolution methods including MC/IC, FTIR, CES and PTR-ToF. Missing data points are results of instrumental issues.

Fire no.	ADS(ppb)	MCIC(ppb)	CES(ppb)	FTIR(ppb)	PTR-ToF (ppb)
8	25.7	25.7	22.4	29.5	29.5
9	21.3	24.9	19.7	--	--
10	42.2	44.2	46.6	--	--
11	112.3	69.8	103.3	--	--
14	25.3	24.5	35.6	25.7	41.3
15	51.0	76.2	58.9	37.9	50.2
16	70.0	56.4	70.1	56.4	--
17	47.1	53.3	39.4	35.1	--
18	45.3	38.3	50.0	41.3	50.0
19	23.8	41.5	28.4	24.3	30.9
20	52.5	42.9	56.8	41.9	--
21	9.9	6.0	--	7.0	16.2
22	40.0	32.0	--	14.5	42.1

Table S3 Data for NOx concentration measured by NOx analyzer and NOx collection system.

Fire #	NO_x_analyzer (ppb)	NO_x_collected (ppb)
2	113.5	147.9
3	151.3	124.7
5	182.7	123.8
6	60.2	94.7
7	313.0	398.3
8	100.5	91.7
9	80.5	73.6
10	156.2	229.7
11	498.9	571.8
12	33.9	36.2
14	39.5	70.0
15	38.9	43.5
16	338.3	443.3
19	84.3	73.3

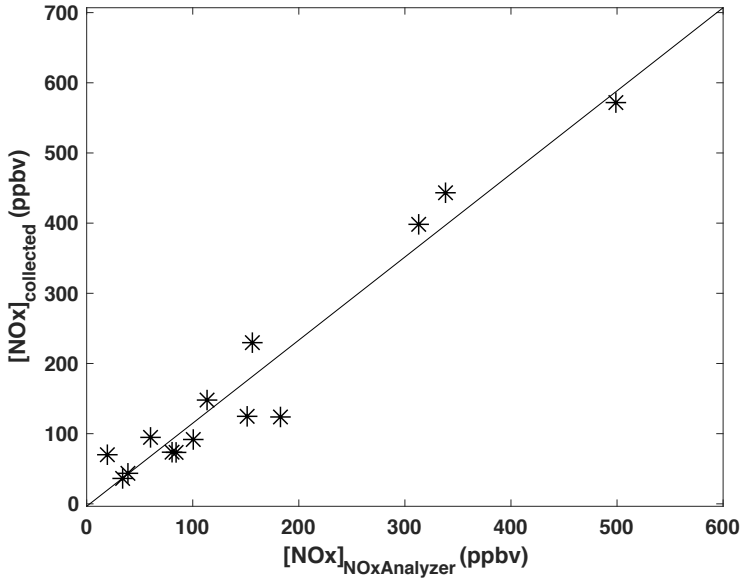

Figure S1 NO_x concentration comparison between NO_x analyzer measurement (mean value over the entire fire) and NO_x collected by the collection system for isotopic

analysis. Solid line is linear regression of the dataset: y = (1.18±0.08)x + (-3.5±17.2), with R^2 = 0.94, p_{slope} < 0.001, $p_{intercept}$=0.84, and uncertainty=1σ.

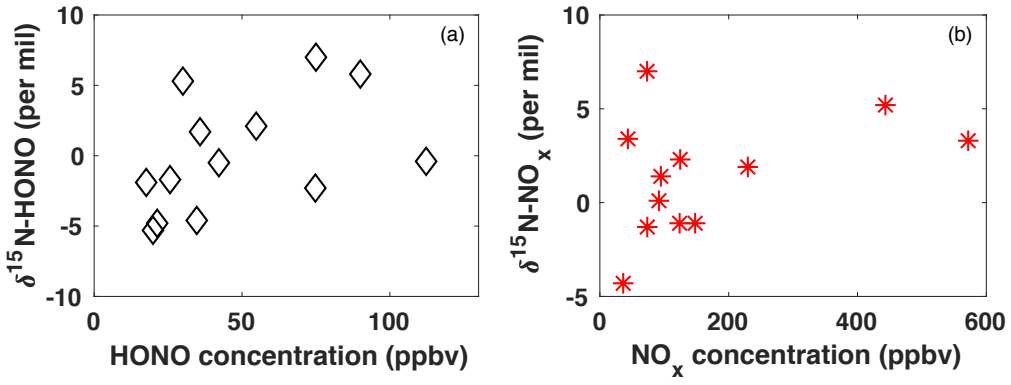

Figure S2. Relationship between $\delta^{15}N$ value versus concentration for HONO (a) and NO_x (b). p-values for linear correlation are 0.12 (a) and 0.93 (b) respectively.

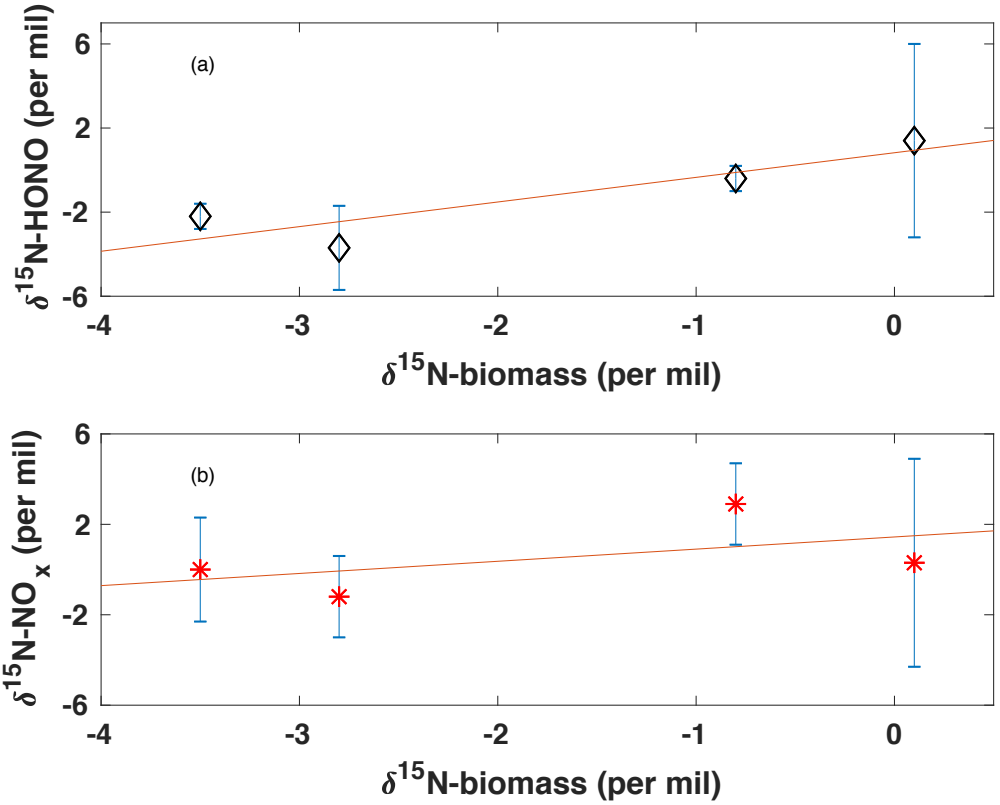

Figure S3. Linear regressions between **(a)** $\delta^{15}N$-HONO and $\delta^{15}N$-biomass, $\delta^{15}N$-HONO = 1.2 $\delta^{15}N$-biomass + 0.80 (r^2=0.83, p_{slope}=0.1), and **(b)** $\delta^{15}N$-NO_x and $\delta^{15}N$-biomass

$\delta^{15}N\text{-}NO_x = 0.54\delta^{15}N\text{-biomass} + 1.4$ ($r^2=0.28$, $p_{slope}=0.5$).
The error bars are propagation of replicate uncertainty (1σ) and method uncertainty.

References

Dunlea, E. J., Herndon, S. C., Nelson, D. D., Volkamer, R. M., San Martini, F., Sheehy, P. M., Zahniser, M. S., Shorter, J. H., Wormhoudt, J. C., Lamb, B. K., Allwine, E. J., Gaffney, J. S., Marley, N. A., Grutter, M., Marquez, C., Blanco, S., Cardenas, B., Retama, A., Ramos Villegas, C. R., Kolb, C. E., Molina, L. T. and Molina, M. J.: Evaluation of nitrogen dioxide chemiluminescence monitors in a polluted urban environment, Atmospheric Chemistry and Physics, 7(10), 2691–2704, doi:https://doi.org/10.5194/acp-7-2691-2007, 2007.

Febo, Antonio., Perrino, Cinzia., Gherardi, Monica. and Sparapani, Roberto.: Evaluation of a High-Purity and High-Stability Continuous Generation System for Nitrous Acid, Environ. Sci. Technol., 29(9), 2390–2395, doi:10.1021/es00009a035, 1995.

FIREX: FIREX 2016 Fire Lab Data Archive, [online] Available from: https://esrl.noaa.gov/csd/groups/csd7/measurements/2016firex/FireLab/DataDownload/index.php?page=/csd/groups/csd7/measurements/2016firex/FireLab/DataDownload/ (Accessed 25 March 2019), 2016.

Koss, A. R., Sekimoto, K., Gilman, J. B., Selimovic, V., Coggon, M. M., Zarzana, K. J., Yuan, B., Lerner, B. M., Brown, S. S., Jimenez, J. L., Krechmer, J., Roberts, J. M., Warneke, C., Yokelson, R. J. and Gouw, J. de: Non-methane organic gas emissions from biomass burning: identification, quantification, and emission factors from PTR-

ToF during the FIREX 2016 laboratory experiment, Atmospheric Chemistry and Physics, 18(5), 3299–3319, doi:https://doi.org/10.5194/acp-18-3299-2018, 2018.

Reed, C., Evans, M. J., Carlo, P. D., Lee, J. D. and Carpenter, L. J.: Interferences in photolytic NO_2 measurements: explanation for an apparent missing oxidant?, Atmospheric Chemistry and Physics, 16(7), 4707–4724, doi:https://doi.org/10.5194/acp-16-4707-2016, 2016.

Selimovic, V., Yokelson, R. J., Warneke, C., Roberts, J. M., de Gouw, J., Reardon, J. and Griffith, D. W. T.: Aerosol optical properties and trace gas emissions by PAX and OP-FTIR for laboratory-simulated western US wildfires during FIREX, Atmos. Chem. Phys., 18(4), 2929–2948, doi:10.5194/acp-18-2929-2018, 2018.

Stockwell, C. E., Yokelson, R. J., Kreidenweis, S. M., Robinson, A. L., DeMott, P. J., Sullivan, R. C., Reardon, J., Ryan, K. C., Griffith, D. W. T. and Stevens, L.: Trace gas emissions from combustion of peat, crop residue, domestic biofuels, grasses, and other fuels: configuration and Fourier transform infrared (FTIR) component of the fourth Fire Lab at Missoula Experiment (FLAME-4), Atmos. Chem. Phys., 14(18), 9727–9754, doi:10.5194/acp-14-9727-2014, 2014.